REACTIVITY, MORPHOLOGY, AND SOLVATION PHENOMENA OVER ELECTRODE INTERFACES IN BATTERY SYSTEMS

A Dissertation

by

KIE SCOTT HANKINS

Submitted to the Graduate and Professional School of
Texas A&M University
in partial fulfillment of the requirements for the degree of

DOCTOR OF PHILOSOPHY

Chair of Committee,	Perla B. Balbuena
Committee Members,	Jeffrey Bullard
	Faruque Hasan
	Jorge Seminario
Head of Department,	Arul Jayaraman

May 2022

Major Subject: Chemical Engineering

ABSTRACT

The global shift towards renewable energy resources and electric vehicles has generated an unprecedented demand for robust energy storage technology. Lithium-ion batteries with graphitic anodes are the current standard of energy storage, but they are insufficient to meet this demand, and are quickly approaching the theoretical limit of their energy density. In order to meet the energy storage requirements of the future, new chemistries beyond the standard lithium-ion formulation are needed. Many new battery chemistries are being researched, but they face substantial challenges in stability and durability that must be overcome before they can replace current technology. These challenges are strongly influenced by the reactivity and morphological behavior of the electrode surfaces, and the ion solvation and transport phenomena that occur in the electrolyte. The reactivity and morphology of the electrode can play both a beneficial or a catastrophic role in battery function, these behaviors are related to the chemical and mechanical properties of the electrode material and the electrolyte. The solvation and transport phenomena of ions control the stability and charging rate, as well as affect the surface behavior of the battery electrodes. These phenomena are influenced by the ion, electrode, and electrolyte chemistries. Much work is being done to understand and mitigate these challenges, but the nanoscale mechanisms that drive them are complex and not well-understood. In this work, I present several projects where I have used primarily-computational methods to elucidate the atom-scale phenomena that occur at electrode surfaces and in the electrolyte, in order to develop a broader understanding of the mechanisms that inhibit future battery chemistries.

DEDICATION

I dedicate this work to my wife Alison, who lovingly feigns interest when I tell her about results in half-jargon, who teaches me and lets me teach her, who stands with me through thick and thin at every point on this grand adventure. Without her support, this would not have been possible.

To my stepfather John, who teaches me how to solve problems big and small, who encourages me to strive towards everything I want in life, who provides a constant example of what it takes to be an honest man.

To my advisor Perla, who helped me grow from an eager child with a love a chemistry, into an eager scientist with a childlike love of chemistry. Her passion for science has inspired me above all others.

ACKNOWLEDGEMENTS

I would like to thank my advisor, Dr. Balbuena, for all of her guidance over these years, and my committee members, Dr. Bullard, Dr. Hasan, Dr. Seminario, and Dr. Murugesan for their collaboration and help during the course of this research.

Thanks also to my friends and colleagues at A&M; Fernando, Leonardo, Samuel, Luis, Ethan, Saul, Stefany, Ryan, and at PNNL; Venky, Grant, Shuttha, Roy, and more, who have been vital help and support throughout my research.

Thank you to the staff in our chemical engineering department, especially Lisa and Ashley, for advising me through my coursework and journey. And for the entire 12th man family of Texas A&M for creating a feeling of welcome and community during my time here.

Thank you to my friends and family, for providing love, support, and much-needed entertainment breaks during difficult times.

Finally, thanks to my wife, Alison, for keeping me grounded through everything, for her patience, love, and excitement.

CONTRIBUTORS AND FUNDING SOURCES

Contributors

This work was supervised by a dissertation committee consisting of Professor Perla Balbuena [advisor], Professor Jorge Seminario and Professor Faruque Hasan of the Artie McFerrin Department of Chemical Engineering, as well as Professor Jeffrey Bullard in the Zachary Department of Civil and Environmental Engineering, and Dr. Vijay Murugesan at Pacific Northwest National Laboratory.

The projects discussed in Chapters 3 and 4 were assisted by many individuals and groups including; The Texas A&M University Departments of Chemical Engineering, Materials Science, Electrical Engineering, and Civil Engineering, the Purdue University Department of Chemical Engineering, the Wright State University Department of Chemistry, the Qatar Environment and Energy Research Group, Sandia National Labs, Pacific Northwest National Laboratory, the Joint Center for Energy Storage Research, and the Air Force Research Laboratory. In order to preserve clarity, the specific contributions will be discussed in detail in the respective sections of each project.

The Texas A&M High-Performance Research Computing center is gratefully acknowledged for the use of their supercomputing resources during the bulk of this work.

Funding Sources

Graduate study was supported by a fellowship from the Texas A&M college of Engineering and Teaching and Research assistantship appointments from the Artie McFerrin Department of Chemical Engineering.

This material is based upon work supported by the U.S. Department of Energy's Office of Energy Efficiency and Renewable Energy (EERE), as part of the Battery 500 Consortium, Award Number DE-EE0008210, and also within the Battery Materials Research (BMR) program, grant DE-EE0007766.

Project with the Pacific Northwest National Laboratory were supported by the Joint Center for Energy Storage Research under the Basic Energy Services program within the United States Department of Energy.

NOMENCLATURE

AIMD	*Ab-initio* Molecular Dynamics
DFT	Density Functional Theory
CMD	Classical Molecular Dynamics
MD	Molecular Dynamics
KMC	Kinetic Monte Carlo
XPS	X-ray Photoelectron Spectroscopy
FTIR	Fourier Transform Infrared Spectroscopy
VASP	Vienna *Ab-initio* Simulation Package
SEI	Solid Electrolyte Interphase
PNNL	Pacific Northwest National Laboratory
JCESR	Joint Center For Energy Storage Research

TABLE OF CONTENTS

Page

LIST OF FIGURES

Page

LIST OF TABLES

Page

1. INTRODUCTION

In this section I will discuss the motivation for research in energy storage technologies, specific energy storage topics and chemistries, and challenges that are posed by these topics and chemistries.

1.1. Need for Energy Storage

The threats of climate change[1] have caused global shift away from fossil fuels and towards renewable energy resources[2–4]. One of the most difficult obstacles to overcome in this shift is the need for robust grid-scale energy storage[5]. The transient nature of renewable energy resources, such as wind and solar, make it difficult to meter the supply of power to cities in order to meet current demand. This is much easier to do with our current fuel-based energy infrastructure; if more energy is needed, more fuel can be burned, and if less is needed then, less fuel is used. This principle cannot be applied to most renewable resources; the sun and wind cannot be intensified to increase power generation to meet high demand, and excess energy would be wasted in times of low demand. Similarly, fuel resources hold energy indefinitely and can be used at any given time, but renewable resources often only produce energy at specific times, such as during daylight and during windy conditions. Grid-scale energy storage technology is needed in order to solve these problems and enable the transition from fuels to renewable energy resources[6–8].

Another large hurdle to cross in the move towards renewable energy is the use of electric vehicles (EVs) in favor of the internal combustion (IC) engine. In order for EVs to be viable, they must have safety and lifetimes comparable to that of current IC technology. They must also be able to supply power for distance ranges that are similar or greater than those of IC technology, and must be able to recharge on a relatively similar timescale to the refueling process of ICs. Current battery technology limits the range of EVs to about 300 miles on a single charge, which allows them to be useful in many cases, but is insufficient for longer and more intense transportation requirements. Improvements in energy density are needed in order to enable the longer ranges required by interstate travel and transport[9,10].

Robust energy technologies, of many different types, are needed to meet the extreme energy requirements of the future; grid-scale storage requires very reliable systems with long cycling endurance; EVs and portable devices require systems with high gravimetric and volumetric energy densities, and resistance to environmental factors. Modern energy storage technology is impressive and rapidly improving, but is still insufficient to meet the demands of a transition away from fossil fuels.

1.2. Current Energy Storage Technology

The current standard of energy storage technology is the lithium-ion battery with a graphitic anode and metal-alloy cathode. This system was a groundbreaking technology that has changed the world over the span of a few decades[11,12]. In spite of this feat, lithium-ion batteries are still subject to several significant issues.

Many Li-ion cathodes contain cobalt and other problematic materials, these chemicals are toxic and pose health and environmental risks[13]. The disposal and recycling processes for the materials in these batteries is tedious and the long-term impacts are not well understood[14]. There are also significant ethical concerns about the use of cobalt as a resource, and the global labor practices that are used to obtain it[15,16].

Lithium-ion batteries have been a major focus of research for decades, and many improvements have been made, to the point where we are approaching the theoretical limit of the energy density of the graphite anode configuration (~372mAh/g)[17]. This capacity, while impressive, is insufficient to meet the energy storage needs of a full transition to renewable energies. If we are to meet the energy storage requirements of the future, new beyond-graphite chemistries and configurations are needed[18].

1.3. Challenges and Popular Research Topics

Energy storage is a popular research topic, and many different chemistries are being actively researched; Li-metal, Li-S, Li-air, Mg-, K-, Ca-, Zn-, and more, are being explored[17,19–23]. Pure Li-metal anodes are often described as the 'holy grail' of energy storage technology because of their incredibly high gravimetric energy density (3860mAh/g) and the low electrochemical potential of lithium. These anodes are subject to several debilitating issues, including instability, uncontrolled surface reactions, lithium loss, dendrite formation, and catastrophic failure, that must be solved before this technology becomes viable. Many other lithium-based and non-lithium technologies are being investigated as 'stepping stones' between current Li-ion technology and this 'holy

grail'. All of these technologies face their own similar challenges, although they are typically less numerous or difficult to overcome than those of lithium metal.

Surface reactivity plays a complex and significant role in the function of a battery. The decomposition of the solvent and electrolyte in contact with the electrode surface creates an array of products that affect how the battery works. For lithium chemistries, this can be beneficial, but for other chemistries such as magnesium, this can be catastrophic. This will be explained further in the next section (**1.3.1**).

Anode materials such as silicon and copper are being investigated as replacements for the standard graphitic material used today[24,25]. These materials have substantially higher capacities than graphite, but undergo swelling and other destructive morphological change during charging. Another phenomenon closely tied to this surface morphology is the formation of dendrites; which cause destructive and often dangerous effects on the battery. A popular field of research is dedicated to understanding these phenomena and their mechanisms, and developing solutions to them; this will be further described in section **1.3.2**.

Many new complex solvent and electrolyte chemistries are being investigated to address the aforementioned problems and enable successful behavior of new battery chemistries. The behavior of these electrolyte systems strongly influences the aforementioned surface reactivity and overall function of the battery. New systems, like lithium-air, have very complex ion transport phenomena that are not well understood. Magnesium-based chemistries face difficulties with solvation and desolvation kinetics and sluggish ion transport because of the complexity of the bivalent Mg^{2+} ion

coordination. Significant work is being done to understand these solvation phenomena and address these issues; this will be further discussed in section **1.3.3**.

1.3.1. The Solid Electrolyte Interphase

The electrode surfaces in battery systems are subject to an array of complex interactions and reactivity with the electrolyte. When these reactions occur, electrolyte species decompose and form a heterogenous layer covering the electrode surface known as the solid electrolyte interphase (SEI). The chemistry and characteristics of this layer are strongly dependent on the chemistries of the electrode, solvent, and electrolyte[26].

This SEI layer is fundamentally important to the stable function of a battery. In lithium-based systems, the monovalent lithium ions are able to easily transport through this layer, and charge cycling of the battery is not disrupted. This layer functions as a protective, or passivating, coating of the surface that inhibits future reactions and significant morphological changes, which extends the stability and cycle-life of the cell[27]. However, if the electrolyte is too reactive, this layer can grow uncontrollably and eventually become too thick for the lithium ions to transport, which stops the battery from cycling[28].

A general understanding of the SEI is well-established[26], but there is still much about the initial formation mechanisms, structure, and chemistries, that is not well-understood. Many studies, including my project discussed in section **3.1** are focused on developing a fundamental understanding of SEI growth and structural characteristics[27,29]. The ultimate goal of these studies is to develop a detailed understanding of SEI

formation that can be used to guide the selection of electrodes and electrolytes to generate of interphases with ideal properties.

Other studies, such as my projects that will be discussed in sections **3.3** and **3.4**, focus on the effect that specific electrode surface and electrolyte chemistries have on SEI generation. These studies seek to both understand the chemistry behind SEI formation[30], and to ultimately use this information to tune the electrode and electrolyte characteristics to create SEI's with desired properties[31].

In magnesium-based systems, the formation of a passivation layer can be catastrophic. It is widely-regarded that the complex interactions of the bivalent Mg^{2+} ion keep it from transporting through even thin passivating layers, and thus render the battery unable to charge cycle[22,32]. There is some recent debate about specific chemistries that allow passivating films to transport Mg^{2+}, acting as an effective SEI [33,34]. Even in these cases, it is agreed that the reactions of the solvent species in the electrolyte form a destructive passivating layer on the surface. Much care must be taken to select an electrolyte that will be less reactive with the electrode surface, and to select species that possible form effect SEI layers in magnesium batteries.

Overall, a substantial amount of battery research is dedicated to tuning and understanding electrolyte and electrode chemistry in order to develop the desired SEI characteristics for the given system[35].

1.3.2. Surface Morphology and Dendrite Formation

The electrode bulks and surfaces in battery systems undergo significant morphological changes during cycling. In most cases, these changes are detrimental to the function of the battery. For instance, in Li-Si batteries, the silicon anode undergoes a volume expansion of up to 400% during charging, this expansion can fracture the SEI and even the bulk structure of the electrode itself, as well as cause larger-scale mechanical issues with the battery[36,37]. Dendrite formation is a closely-related issue; during charging, cations can deposit and agglomerate in the electrode surface. If these agglomerations continue to grow, they form structures called dendrites, which can generate significant issues with battery function. These dendrites can break at their base and become disconnected from the circuit, creating 'dead lithium' that do not participate in cycling and thus cause capacity loss. If these dendrites continue to grow and do not break, they can pierce the membrane separator and reach the counter electrode of the system, causing a short circuit and catastrophic failure of the battery[17,38].

The elucidation of the underlying mechanisms behind these morphological changes and dendrite formation is an active area of research. Another branch of research is focused on modifying the components of battery systems in order to combat the detrimental effects of these phenomena. There are many different ways to combat these issues, including artificial surface coatings and SEI's, electrode surface structuring, and new electrode and electrolyte chemistries.

Recent advancements in atomic deposition techniques and polymer chemistry[39] have created a strong interest in the development of artificial surface coatings to protect

the electrode surface and inhibit dendrite formation and morphological. Many types of artificial surface layers ranging from polymers[40] to complex nanoparticles[41], are being investigated as a means to guide uniform lithium deposition and avoid dendrite formation in lithium metal batteries. Other coatings care designed stabilize the electrode structure by reversibly expanding and contracting with the electrode during the swelling induced by charge/discharge cycles in lithium-silicon batteries[42,43]. The nanoscale phenomena that occur at the interfaces of these coatings and the electrode during cycling are complex and not well-understood; my project discussed in section **3.2** investigates these phenomena.

Recent advances in nanoengineering have inspired many nanostructured electrode configurations designed to efficiently and stably intercalate ions. These designs intend to direct homogeneous cation deposition to either allow for stable electrode growth without fracture[44], or to inhibit the initial surface agglomerations that eventually form dendrites[45]. Some of these structured electrodes have shown promising results, but morphological changes can destructively disrupt these structures[46,47]. This nanostructuring is relatively novel field, and a greater understanding of the nanoscale deposition behavior is needed to guide future study and designs, my projects discussed in sections **3.5** and **3.6** are focused on developing this understanding.

1.3.3. Solvation and Desolvation Behavior

The solvation and desolvation processes of ionic species between the electrolyte and electrodes in battery systems are influenced by a complex combination of the

electrode material, the electrolyte chemistry, and the coordination characteristics of the ion. These processes dictate the ionic mobility in the system and thus the overall charge transfer behavior of the cell in all battery chemistries, they can also influence the electrode surface and bulk through desolvation and solvation behavior. These processes are particularly complex and important in Mg-based chemistries and lithium-air batteries.

The solvation behavior of Mg-based batteries is a difficult problem to understand and overcome for two main reasons, both of which are mainly influenced by the strong interactions of the Mg^{2+} ion. First, the ion-electrolyte-solvent coordination structures are complex and relatively large. And second, the Mg^{2+} ion is resistant to desolvation out of these coordination complexes and into the electrode, which leads to sluggish dynamics and charge transfer. This complex solvation behavior, coupled with the constraint of requiring unreactive species, makes it difficult to find effective electrolyte systems for Mg-based batteries. New solvent and electrolyte combinations are being actively investigated, some with promising results[48], but the underlying mechanisms of their behavior are not well-understood. Further studies are needed in order to guide the search for successful electrolytes[48,49], my project discussed in section **4.2** investigates one such system.

Li-Air batteries function significantly differently than standard battery technology. They possess a very high gravimetric energy density because, in place of a standard cathode, a small electrode is used with ambient air to reduce the cation during discharge; this lack of a cathode substantially lowers the overall weight of the system

and thus increases the energy density. There are several challenges that these batteries face, one of which is the requirement of a complex solvation process to transport and reduce the ambient oxygen[50].

The underlying processes that power lithium-air batteries present a unique and difficult challenge in solvation phenomena. The final product of the redox reactions that these batteries are based on, Li_2O_2, is an insoluble solid, and will deposit on and insulate the electrode, inhibiting further charge cycling. In addition, the superoxide $[O_2]^-$ species is a suspected intermediate in this reaction, and is chemically destructive to the rest of the battery components[50–52]. The use of transport molecules designed to reversibly carry the reaction intermediates to and from the cathode, so that the insoluble species can be deposited elsewhere, is an area of active investigation. These catalysts also have the potential to contain the dangerous superoxide species[53]. The underlying mechanisms behind this catalytic transport are not well-understood, and a detailed understanding of the solvation phenomena is needed to inform future work. My project discussed in section **4.1** discusses the properties and mechanisms of a novel Li-air catalyst.

2. METHODOLOGY

Computational methods are invaluable for elucidating phenomena that occur on time- and length-scales too small or precise to be observed with experimental techniques. I have used a variety of primarily-computational methods throughout my research. In this section, I will discuss the theory that powers each of these methods and then discuss their practical implications and uses. I will briefly provide more specific methodology for each project discussed in Chapters 3 and 4.

2.1. Density Functional Theory

Density Functional theory (DFT) methods are known as *Ab-initio*, or 'first principles' methods. They do not require any system-specific parameterization, and are incredibly precise compared to other computational methods. DFT methods are based on solutions to the Schrodinger's equation[54] and use quantum mechanical modeling to represent the electronic behavior of a system with functionals (functions of functions)[55]. The basis of these functions are Schrodinger-like wave equations, which are combined with many theorems[56–58] and approximations in order to make them solvable on a practical timescale. These equations are solved for the spatially-dependent electron density of the system; this dramatically reduces the numerical complexity of the calculations, and is the basis of Density Functional Theory. The electronic density and atoms (called 'ions' because they are separated from their electrons) are treated as separate entities, and their respective energy and force potentials are calculated individually, then these potentials are coupled together and the net contributions are

solved for iteratively. The theory that powers DFT methods is robust, but does have limitations in specific systems and computational cost, and improvements are being actively researched[59–62].

The two driving forces behind DFT calculations are the type of functional used and the basis set that is applied to it. The functional makes up the guiding equations for the system, and the basis set describes the extent to which the functional is applied. In simple terms, one can think of the functional as corresponding to accuracy and the basis set corresponding to precision. The majority of the driving terms behind DFT functionals are exact, but the two terms relating to the exchange and correlation energies from quantum effects are not. There are many functionals that approximate these terms in different ways, but there is no exact universal solution. Some functionals are better for certain chemistries than others, and some knowledge and intuition is required when selecting a functional for a given system[63,64]. Basis sets loosely correspond to the atomic orbitals that the functionals are applied to[65,66]. Many different basis sets are available, and their selection is based on the type of functional, level of precision, and characteristics of the calculation being performed.

2.1.1. Orbital-type DFT

DFT methods can be split into two distinct categories: orbital-type, and plane-wave type. Orbital-type methods use electronic functionals that are centered around the nucleus of their respective ions and take the shape of orbitals[67–69]. These methods can be further split into Slater-type orbitals[70,71] and Gaussian-type[72,73] orbitals. Slater orbitals

are more physically representative of the true electronic behavior, but are computationally expensive. Gaussian-type orbitals are more-commonly used; they are significantly faster than Slater-type, and although they are not as physically representative of real systems, approximations and additional care can be taken to make them just as accurate.

Gaussian 09 and 16[74] and Amsterdam Density Functional (ADF[75,76]) are examples of software packages that implement orbital-type DFT. They are useful for studies focused on non-periodic molecular structures and can be used to obtain geometry, atomic charge, spectra, energies, and barriers. All orbital-DFT atomic charges presented in this work are calculated using the Mulliken method[77,78]. Practically, orbital-type DFT calculations are limited to the scale of tens of atoms. I have used both Gaussian and ADF to perform all of these calculations for many different systems throughout my work.

2.1.2. Plane-Wave DFT

Plane-wave basis sets allow for less-localized treatment of the electronic structure, and are typically used for systems with periodic boundaries, such as solid surfaces and interfaces. In most plane-wave systems, only the valence electrons of the atoms are treated explicitly, the core electrons are treated as part of the ion itself, and their effects are paired with the ion to represent a net force field, called a pseudopotential[79,80]. Another significant part of plane-wave DFT is the use of k-points. In some cases, the phase of the periodic potential wavefunction extends across the

periodic boundary beyond the simulation cell, typically with smaller cells. One must specify how far to carry the integration of the wavefunction across the boundary in order to obtain accurate results, the k-points are the values used to describe that[81].

I have used the Vienna *Ab-initio* Simulation Package (VASP)[82] versions 5.3 and 5.4 for all of my plane-wave DFT calculations. It is useful for calculating geometries and structure, system and event energies, atomic charge, and spectra of systems related to surface phenomena. All plane-wave DFT atomic charges presented here are calculated using the Bader method[83,84]. The computational cost of plane-wave DFT is relatively large, and limits these calculations to a few hundred atoms.

Unless otherwise noted, the system parameters for all VASP DFT calculations performed in this work are described here. These calculations employ the PBE[85–87] functional within the Generalized Gradient Approximation (GGA). The cutoff energy for the planewave basis set is set at 400eV[88]. Ions and core electrons are represented with the PAW pseudopotentials included in the VASP package[80,89].

2.2. Ab-initio Molecular Dynamics

Ab-initio Molecular Dynamics (AIMD) can be thought of as an extension of DFT into dynamic systems. DFT functionals for electronic potential are combined with pseudopotentials for the ions to generate the energies and forces acting on each body in the system, these forces are then used to update the positions and velocities relative to a provided timescale (typically 1 femtosecond)[90,91] by integrating Newton's 2nd law of motion. Most calculations are performed with the canonical, or NVT, ensemble, where

the number of moles, volume, and temperature, are kept constant. The temperature of the system is controlled with a thermostat, such as the Nosé Hoover[92] thermostat, that scales the velocities of the atoms in the system periodically at each step.

I have also used the VASP 5.3 and 5.4 versions for all of my AIMD calculations, it is useful for determining electron transfer and atomic charge, reaction structures, interfacial activity and reactivity, solvation structures and coordination, surface and near-surface behavior. It can also be used with applied geometric constraints to generate energy barriers for events and reactions. AIMD is very expensive and is limited to a few hundred atoms on the picosecond timescale.

Unless otherwise noted, the system parameters for all VASP AIMD calculations described in this work are the same as those listed in section **2.1.2**. In most AIMD calculations that include solvent or significant amounts of species with intermolecular interactions, I employ the DFT-D3 correction method for dispersion forces[93]. In addition, in all AIMD calculations, hydrogen is treated with a tritium mass so that a one femtosecond timestep may be employed.

2.3. Classical Molecular Dynamics

Classical molecular dynamics (CMD) is a very broad and useful technique focused on studying the trajectories of atomic and molecular species. It is based on Newtonian equations of motion that are applied to parameterized atomic force fields on each species in the system, these are often combined with coulombic and Lennard-Jones interactions[94–96]. Since the atomic force fields are parameterized for specific systems,

this is not an *ab-initio* method. Bonds are unbreakable and treated as springs with harmonic force constraints on their length, angles, and dihedrals[97]. The inter- and intramolecular parameters for these simulations are obtained from experimental data and/or ab-initio calculations. The temperature and pressure of these simulations are often controlled by thermostats that direct the velocity of the atoms and the size of the simulation box[92]. Electrons are not represented explicitly and thus it is not feasible to get information on charge transfer between species[98]. There are many types and levels of force fields and parameters that can be applied to CMD systems, which direct how precise and how computationally expensive they are[99].

I have used the Large-scale Atomic/Molecular Massively Parallel Simulator (LAMMPS[100]) for all of my CMD calculations. It is useful for obtaining solvation data, clustering analysis, surface morphology, and thermodynamic properties. It is much less expensive than *ab-initio* methods, and can be used for systems with tens of thousands of atoms on the nanosecond timescale.

2.4. Kinetic Monte Carlo

Kinetic Monte Carlo (KMC) is a coarse-grained simulation method suited to larger time- and size- scales than the previously discussed methods[101,102]. This method is based on the Monte Carlo algorithm, and is based on using iterative random sampling to obtain probabilistic data. KMC is one of the oldest simulation methods, and has been applied to many fields, from quantum to macroscopic scales[103].

In this method, an initial system configuration and chemistry is defined, and the types of possible events in the system are tabulated with their respective rates. At each simulation step, all possible reactions and rates are calculated and a random number is generated and combined with the cumulative rate of the system to determine the given event that will occur during that simulation step. The effects of this event are then applied to the system, and the process repeats. Timescales are calculated based on the rate of the event that occurred[104–106]. Results from these simulations have been shown great accuracy in reproducing realistic timescales and behavior, as long as the provided rates are accurate[107].

The input reaction rates are obtained from experimental data and/or finer-grained simulation methods. One of the largest drawbacks of KMC is that it cannot predict new events; the behavior of the system is limited to what is specified in the inputs. In spite of this limitation, this method is very effective at predicting the time-dependent changes and evolution of systems where the ongoing processes are well-known, and can be applied over time and size-scales far beyond that of other simulation methods.

2.5. System Construction and Analysis

Unless otherwise indicated, all initial systems for DFT and AIMD calculations were constructed using the Biovia Materials Studio Suite[108]. Crystal structure data was obtained from the Materials Project[109]. CMD systems were constructed with the assistance of the PACKMOL[110] and Moltemplate[111] software packages.

Visualization and analysis of computational systems were performed using the OVITO[112], VESTA[113], and VMD[114] software suites. Peak-fitting and analysis of XPS data was performed using the CasaXPS[115] software package. Graphic and numerical analysis were performed with Microsoft Excel[116] and Origin[117].

2.6. X-ray Photoelectron Spectroscopy

X-rat Photoelectron Spectroscopy (XPS) is the only experimental method I have used directly for my work. It works by bombarding a surface with x-rays and measuring the quantity and kinetic energy of electrons that are subsequently emitted from this surface[118,119]. These measurements are often paired with ion-bombardment of the surface in order to remove surface oxides and contaminants. This is a very precise method, it can determine both qualitative and quantitative nanoscale characteristics of a surface, up to a few nanometers deep. XPS measurements must be performed at ultra-high vacuum conditions, which allows for a pristine and precise surface to be used[118]. The data must be charge-corrected to standardized values and then data peaks must be curve-fitted to identify precise binding energies using software such as CasaXPS[120] software package. The binding energies observed in these measurements are compared to known values[121] in order to identify the compounds present on the surface.

3. THE SOLID ELECTROLYTE INTERPHASE AND SURFACE REACTIVITY

This chapter of my work is concerned with the surface phenomena on the electrodes of battery systems. These surfaces are subject to substantial amounts of reactivity and morphological change during the normal cycling operation of the electrochemical cell. These complex phenomena play significant roles, both beneficial and detrimental, in the performance and lifetime of the battery, and understanding their mechanisms and behavior is a fundamental step in improving the chemistry of the battery.

3.1. [*]Unveiling the First Nucleation and Growth Steps of Inorganic Solid Electrolyte Interphase Components[122]

I began this project as an undergraduate student, and it was the first project I completed during graduate school in 2018. In this project, we examined the initial nucleation and growth behavior of two common lithium-ion battery SEI components, LiF, and Li_2CO_3. As discussed in section **1.3.1**, the characteristics of the SEI have a significant effect on the behavior and cycle-life of the battery; understanding the initial stages of their formation provides valuable insight on the overall behavior of the SEI, and serves as a starting point for developing artificial SEIs with desired

[*] Reprinted with permission from "Unveiling the First Nucleation and Growth Steps of Inorganic Solid Electrolyte Interphase Components" by Asma Marzouk, Victor Ponce, Laura Benitez, Fernando A. Soto, Kie Hankins, Jorge M. Seminario, Perla B. Balbuena, and Fedwa El-Mellouhi, 2018. J. Phys Chem. C, 122, 25858-25868, Copyright 2018 by American Chemical Society.

characteristics[123]. Prior models indicated that a fully developed SEI consists of a dense inorganic layer near the electrode surface coated with a semi-porous layer of decomposed organic components[124–126]. In this study, we were able to describe the initial growth pathways of LiF and Li_2CO_3 SEI components, and confirm the morphology of the inner layer of the SEI.

The first mode of this experiment used DFT gas-phase calculations to examine the energies and geometries of LiF and Li_2CO_3 added group-by-group (Figure 1a and 1b) guided by the structure prediction algorithm USPEX[127,128]. The initial calculations and structure predictions were performed in VASP, and the most stable structures observed in these calculations were subjected to further optimization and analysis in the Gaussian DFT program using the PBE/HSE06[129] functional with a 6-311+G basis set[68]. Lastly, single-point calculations of the clusters exposed to gold electrodes[130] were performed with the B3PW91[131] functional and a 6-31G(d) basis set, where the electron transfer properties were observed under applied voltage.

The growth pathways of the most stable, as well as closely (within 200meV) metastable, clusters were followed and their energies were observed. Many of the geometries observed were in agreement with previous studies[132], but some of the metastable growth modes generated novel and unexpected structures that were relatively stable. In most cases, the most stable cluster geometries were crystalline and/or cage-like in structure, rather than amorphous, indicating that even the initial stages of the SEI are likely to be stable crystalline structures. Both LiF and Li_2CO_3 formed highly stable structures where the energy/atom decreased, approaching the value of the bulk material,

as the size of the cluster increased. These results indicate a possible SEI nucleation mechanism where the presence of intermediate metastable clusters provide active areas for new monomers to nucleate.

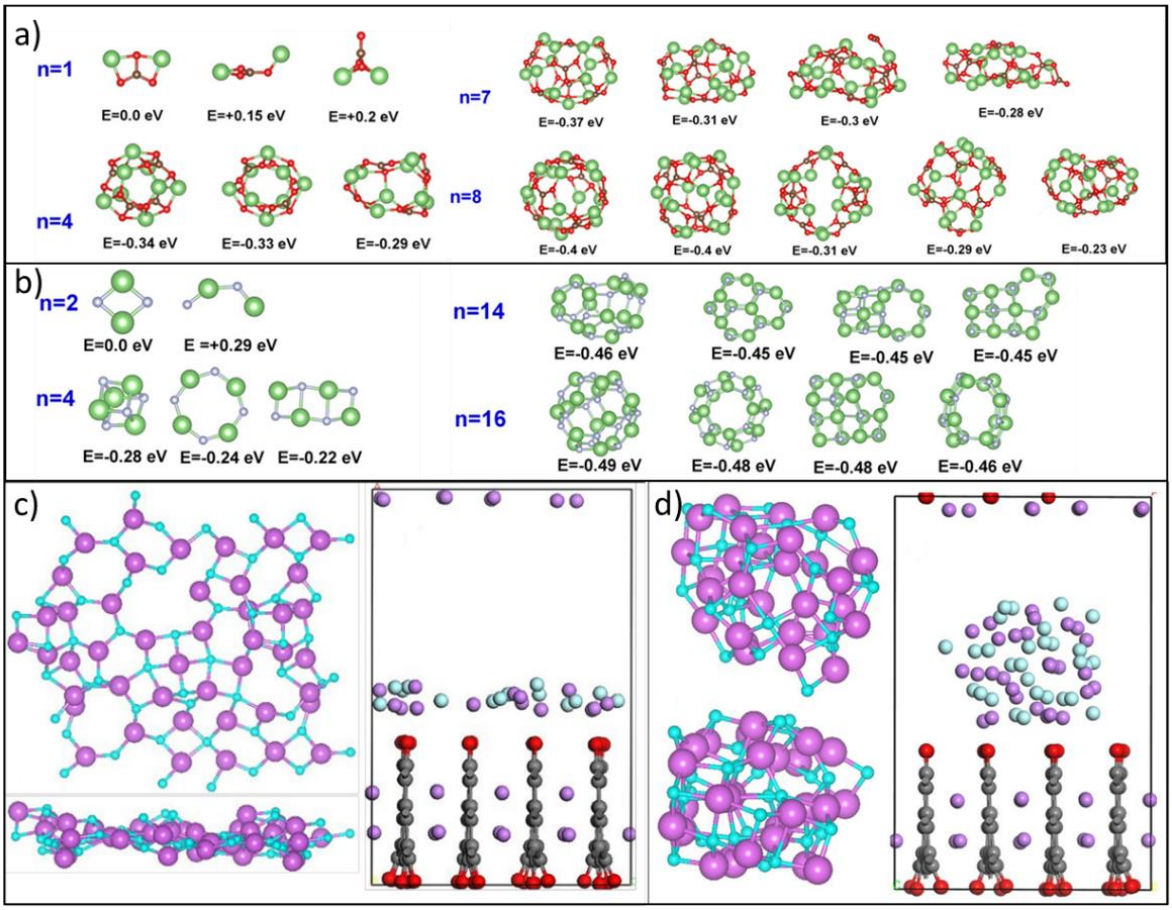

Figure 1. Gas Phase growth of Li_2CO_3 (a), and LiF (b), Li are shown in green, O in red, C in brown, F in blue. Layer (c) and Cluster (d) Growth of LiF on O-terminated graphite, Li are shown in purple, C in grey, O in red, F in blue. Reprinted with permission from "Unveiling the First Nucleation and Growth Steps of Inorganic Solid Electrolyte Interphase Components"

The second mode of this experiment examined the effect of the electrode surface chemistry on the nucleation behavior of these clusters. We created several fully-lithiated graphitic surfaces with, un-terminated ends, and with partial hydration and oxidation.

We then used VASP to preform DFT geometry optimizations of the surfaces, then deposited the ionic species on top of these surfaces and calculated the geometry and energy of each step. We investigated three methods of nucleation, whole-cluster deposition, pairwise layer-based growth, and pairwise cluster-based growth (Figure 1c and 1d). The adsorption locations were determined using the Adsorption Locator function in the Biovia Materials studio calculations.

On non-passivated graphite surfaces, larger clusters exhibited noticeably more favorable adsorption compared to smaller ones, but no trends were observed for H-terminated graphite. Clusters with open-cage structures exhibited more favorable adsorption than those with closed geometry, likely because of the higher concentration of active sites. When LiF were deposited in the layer-growth mode, a defective crystal structure was formed, likely due to destabilizing interactions from the graphite surface. This phenomenon has been previously observed and is corroborated here[133]. The pairwise adsorption energy decreased as more pairs were added, and plateaued to about -2.5eV/pair, this same trend was observed for the cluster-growth mode. This similarity in energy indicates that the initial stages of the SEI are likely to be a heterogeneous mixture of both layered and clustered structures. The adsorption of Li_2CO_3 exhibited a propensity to form a stable overlayer on the electrode surface, where the pairwise adsorption energy plateaued until a layer was complete and a new layer started to form. The overall behavior of Li_2CO_3 nucleation indicates that as the SEI becomes thicker, the outer layers of the film will become less dense.

This work contributed to the overall understanding of monomer nucleation mechanisms and the initial stages of SEI growth. We were able to propose a model for monomer nucleation based on the presence of active sites on metastable clusters. We were also able to elucidate the properties of the initial layering and clustering structures of the SEI.

This was a collaborative work with Dr. Balbuena's and Dr. Seminario's groups at the Texas A&M University Department of Chemical Engineering and Drs. El-Mellouhi and Marzouk at the Qatar Environment and Energy Research Institute. Dr. Soto and I performed the surface DFT calculations. Victor Ponce, Asma Marzouk, and Laura Benitez performed gas-phase calculations.

3.2. †Chemical and Mechanical Degradation and Mitigation Strategies for Si Anodes[134]

This project was started during my undergraduate degree, and was the second project I completed during my Ph.D. studies. In this work, we examined the chemical and mechanical degradation of Li-Si anodes and their SEI's, and the behavior of artificial surface coatings that have been proposed to mitigate this degradation. Silicon is a very promising anode material candidate for next-generation lithium-based batteries because it can intercalate a high amount of Li per Si (up to $Li_{4.4}Si$), which provides a

† Reprinted with permission from "Chemical and mechanical degradation and mitigation strategies for Si anodes" by Diego E. Galvez-Aranda, Ankit Verma, Kie Hankins, Jorge M. Seminario, Partha P. Mukherjee, Perla B. Balbuena, 2019. Journal of Power Sources, Volume 419, 208-218, Copyright 2019 by Elsevier

massive theoretical charge capacity of up to 4200 mAh/g[135]. This high lithium intercalation capacity is accompanied by a large volumetric change, up to 400%, during charge cycling, which causes catastrophic damage to the electrode and the SEI layer[24,136]. There are many studies focused on developing a better understanding of this volume expansion and its damage modes[137,138], as well as ways to avoid this damage, such as nanostructured electrodes[139,140] or surface coatings that can expand and contract elastically[36,141]. In this study, we use atomistic and mesoscopic modeling to observe the failure modes of lithium-silicon anodes during volumetric expansion, and AIMD to examine the interfacial reactions and morphology of artificial surface coatings that have been proposed to mitigate the damage caused by this expansion.

The first stage of this work used a mesoscopic lattice spring model[142] consisting of a particle with a core of active silicon material coated with a surface film. The active material was studied with two different configurations; amorphous and crystalline. Diffusion was modeled with Fick's law for one-phase[143], and Cahn-Hilliard for two-phase[144].

The next stage of this work used a molecular dynamics atomistic model of a 4.4nm $Li_{3.5}Si$ nanoparticle coated with a 1.8nm thick LiF SEI layer. A time-dependent LJ expanding potential[145] was used to simulate the volume expansion of the particle during charging, and this potential was changed to study the effect of different charging rates.

The atomistic model predicted the onset of volume expansion to begin at a Li concentration that corresponds to 10% of maximum lithiation. This data corroborated

what was observed with the mesoscopic model and previous work. The rate of volume expansion in the particle was observed to be almost linear with respect to lithium concentration. At higher concentrations the trend deviates from this linearity and behaves more as a function of charge, with asymptotic behavior. The particle was subjected to several different charging rates in order to observe the effect on the system. The damage density (ratio of broken bonds and initial bonds) was used as a metric to quantitively track the damage to the nanoparticle during expansion. It was observed that higher charging rates caused higher damage densities, but did not cause fracturing of the cluster, because the rapid change caused the crystal structure of the particle to become amorphous. In general, less amorphization occurred with lower charging rates. For lower charging rates, the damage density was lower and occurred more slowly, but large fracturing of the SEI was observed (Figure 2b). The damage density at the point of fracture was observed to be a function of the charging rate, suggesting that there is a minimum threshold for damage density in the particle.

Another significant observation during these simulations was the emergence of phases of different Li concentration within the nanoparticle, and notable interfaces between these phases. This behavior corresponds to the two-phase alloying behavior of silicon electrodes. The interfaces of these phases mark points of high tensile stresses in the particle, which contribute to significant mechanical damage. This problem was not observed in amorphous silicon clusters because the amorphous structure allowed for single-phase diffusion.

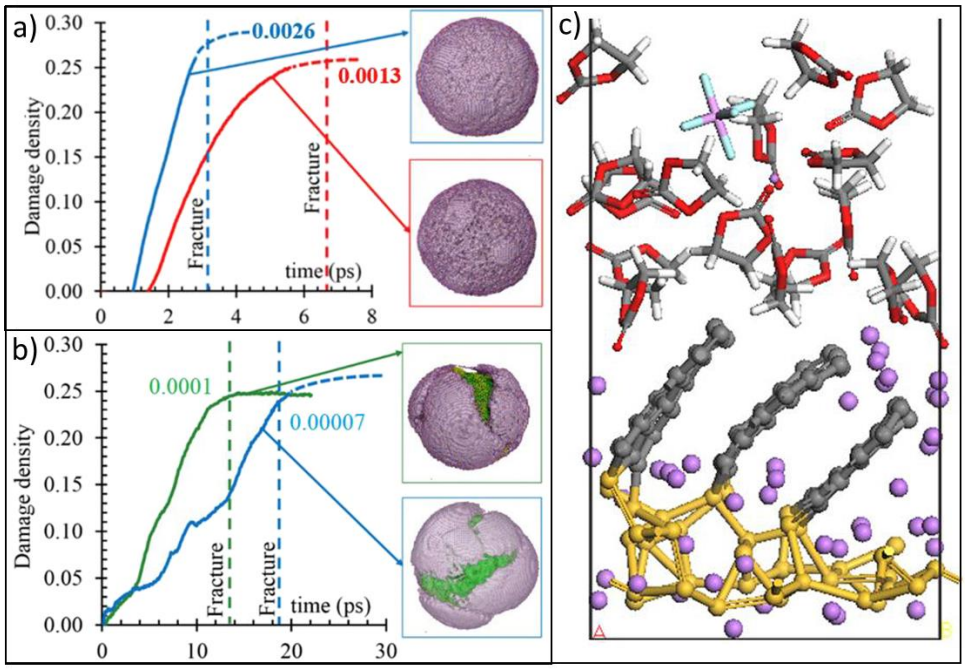

Figure 2: a) Damage density of Si Cluster at high charge rates. b) Damage density and SEI fracture at different low charge rates. c) LiSi anode coated with graphene sheets under EC and $LiPF_6$, after full lithiation. C are shown in grey, H in white, O in red, Li on purple, Si in yellow, F in blue, P in pink.

Reprinted with permission from "Chemical and mechanical degradation and mitigation strategies for Si anodes"

Mesoscopic calculations indicated that fracturing of the SEI was much more prevalent than fracturing of the particle during volume expansion, and that capacity loss in these systems is mostly attributed to this SEI fracture. The opposite behavior was observed during the volume reduction of discharging, where the tensile stresses caused more strain on the surface Si than the SEI film. These sections of the study provide significant insight on the mechanisms and consequences of volume expansion during lithium stripping and plating.

The final stage of this work used AIMD modeling of Li_1Si_1 anodes at 400K with three different coatings; graphene, reduced graphene oxide, and a self-healing polymer (SHP) proposed by Wang et. al[36]. These surfaces were coated with ethylene carbonate and 1M $LiPF_6$, lithium atoms were inserted into the electrodes at regular intervals during dynamics. Helium atoms were placed with fixed positions at the top of the cell in order to limit interactions across the periodic boundary. For the SHP simulations, a 0.5fs timestep was used to allow for the use of a standard hydrogen mass in order to better-represent the self-healing bonds, which are based on hydrogen bonding interactions. Additional DFT calculations were performed on sections of the SHP using Gaussian with a M06-2X functional and 6-311++g(3d,3p) basis set. It is important to note that the time-and size-scales of AIMD limit how much of the film behavior we can observe, but these calculations still provide valuable insight on the surface-film interactions.

Significant bonding between the graphene/graphene oxide and the LiSi surfaces was observed during the AIMD calculations. The graphene sheets all oriented near-perpendicular to the surface and bonded at the base (Figure 2c), the reduced graphene oxide sheets bonded to each other and formed a bowl-shaped structure attached to the electrode at its base. This behavior indicates strong adhesion between these coatings and LiSi electrodes. No reactions or electrolyte decomposition were observed in the system with graphene sheets. The reduced graphene oxide reacted with one ethylene carbonate species and also self-reacted to produce a single CO_2 species, indicating that it is not as chemically stable of a surface film compared to pure graphene. This is still an important chemistry to study because it is difficult to obtain a pristine surface coating, and the

reduced graphene oxide gives us insight on the behavior of a graphene coating that has oxidized contamination. Other studies noted significant reactivity using the same electrolyte and electrode chemistries on the same timescales as the calculations performed here[146], indicating that these coatings are effective at reducing reactivity and increasing surface stability.

The 'self-healing' properties of the SHP stem from extensive hydrogen bonding along the backbone of the polymer, as well as from specially-designed hydrogen bonding sites that are added periodically throughout the polymer chain. These hydrogen bonds are expected to easily break and reform to account for the expansion of the Si electrode. AIMD calculations of the LiSi surface coated with this SHP showed significant reactivity; $LiPF_6$ salt decomposed before any additional lithium were inserted, and reactions of the polymer chain, consisting of N-N bond cleavage and self-reaction to form a 3 membered C-N-C group, and reactions with the electrode surface, were observed after lithium insertion. Lithium ions were observed interacting with the hydrogen-bonding sites during dynamics, DFT calculations were performed to further investigate this behavior. We observed that the lithium atoms had mild interactions with the hydrogen bonding sites, but a single lithium ion was able to fully coordinate to these sites and break all of the hydrogen bonds. All of these calculations indicate a dynamic and possibly troubling behavior of the polymer during lithiation/delithiation that should be investigated in future studies.

Overall, this project provided significant insight into the failure mechanisms of volumetric expansion in LiSi anodes. We were able to determine relationships between

failure, morphological changes, and charging rates, as well as the nanoscale consequences of these phenomena. We were also able to investigate the first stages of developing artificial surface coatings to mitigate these problems, and provide insight to guide future study.

This was a collaborative work with Dr. Balbuena's and Dr. Seminario's groups at the Texas A&M University Department of Chemical Engineering and Dr. Mukherjee at the Purdue University School of Mechanical Engineering. Mesoscopic calculations were performed by Ankit Verma, atomistic calculations were performed by Diego Galvez-Aranda, and I performed the AIMD and DFT calculations.

3.3. ‡Role of Polysulfide Anions in Solid-Electrolyte Interphase Formation at the Lithium Metal Surface in Li–S Batteries[147]

This was my primary project while at an internship at the Pacific Northwest National Laboratory. In Li-S batteries, polysulfide species in the cathode dissolve and shuttle to the anode, where they react with the surface and impact the formation of the SEI and cycling of the battery[23,148]. The behavior of these surface reaction mechanisms, as well as the general redox behavior of individual species on well-defined battery surfaces, is not well-understood due to the complexity of these systems[149,150]. Sulfur is an effective probing species to study general redox chemistry because it can easily

‡ Reprinted with permission from "Role of Polysulfide Anions in Solid-Electrolyte Interphase Formation at the Lithium Metal Surface in Li–S Batteries" by Kie Hankins, Venkateshkumar Prabhakaran, Sungun Wi, Vaithiyalingam Shutthanandan, Grant E. Johnson, Swadipta Roy, Hui Wang, Yuyan Shao, Suntharampillai Thevuthasan, Perla B. Balbuena, Karl T. Mueller, and Vijayakumar Murugesan, 2021. J Phys. Chem. Letters., 12, 9360-9367, Copyright 2021 by American Chemical Society.

oxidize or reduce to a range of oxidation states. In this work, we used a combined experimental and theoretical approach to understand the reduction and oxidation reactivity behavior of polysulfide species on lithium metal surfaces. Ion Soft Landing[151] (ISL) was used to deposit a uniform species onto sputter-cleaned lithium-metal surfaces, transfer and analysis of these surfaces was performed *in situ* in order to develop an understanding of the pristine and isolated chemistry of a single species on a chemically controlled surface. AIMD calculations of several lithium-based surfaces were performed in order to develop an understanding of the atom-scale reaction pathways that occur in these systems.

XPS measurements were performed with a Kratos Axis Ultra DLD spectrometer, which employs a high-performance Al Kα monochromatic X-ray source (1486.6 eV, 150 W). Lithium-metal substrates were initially cleaned by Ar^+ sputtering under ultrahigh vacuum conditions in order to remove surface contaminants. In spite of these cleaning conditions, surface oxides (72.8%) and carbonates (~1%) still remained on the surface; the extreme reactivity of Li metal allows it to oxidize even at ultrahigh vacuum conditions. These surfaces are still representative of how lithium-metal would exist in a battery system. The cleaned surfaces were transferred *in vacuo* to the ISL system, where LiS_4^- anions where deposited onto the surface. ISL allows for a very controlled and uniform deposition of materials, closely corresponding to a monolayer. The surfaces were transferred *in vacuo* back to the XPS chamber, and *in situ* analysis of the surfaces was performed. CasaXPS software was use to correct the data to the Li_2O O 1s peak at 528.5eV, and peak fitting was performed with 70%Gaussian/30%Lorentzian curve

shapes and peak identification was performed with the NIST XPS database[121] and data from Laing *et al*.[152], and Seh *et al*[148].

The XPS analysis revealed the presence of both reduced and oxidized sulfur species on the lithium surface. Peaks corresponding to Li_2S (-2), Li_2S_2 (-1), SO_3^{-2} (+4), and SO_4^{2-} (+6) were all observed, and are shown in Figure 3e. Peaks corresponding to the initial anion, elemental sulfur (+0), and terminal sulfur (-1), showed concentrations of 0% and 2%, respectively, indicating almost complete and irreversible reaction of the deposited species. The dominant sulfur-containing species on the surface were SO_4^{2-} (48.9%) and S^{2-} (41.1%), with the remaining being mostly SO_3^{2-} (8.5%). The main two components indicate that the LiS_4^- anion readily follows both reduction and oxidation pathways, and preferentially undergoes full reaction to form fully reduced or oxidized species. The majority of the products were oxidized species (~57.4%), which indicates that oxidation is the more favorable pathway and is a multistep process, it also possibly indicates that full oxidation might be limited by the availability of oxygen on the surface. The low presence of S^- indicates that Li_2S_2 formation is essentially an intermediate on the path to the full reduction product Li_2S. XPS imaging showed that reduced and oxidized species nucleated primarily in different regions, with about 20% overlap of phases with coexisting species. The governing reactions for the formation of the dominant species based on the LiS_4^- bridging sulfur, S_b^0, were determined to be:

1) $4Li_2O + S_b^0 \rightarrow SO_4^{2-} + 8Li^+ + 6e^-$

2) $3Li_2O + S_b^0 \rightarrow SO_3^{2-} + 6Li^+ + 4e^-$

3) $2Li^0 + S_b^0 \rightarrow Li_2S$

The surfaces studied in the experimental portion of this work consisted of a heterogeneous combination of lithium -metal, -oxides, -sulfides, -carbonates, -hydroxides, and -halides. AIMD calculations were performed of Li_2S_4 species on each of these individual surfaces in order to isolate and correspond the experimentally observed reaction products to their respective surface chemistries, as well as to develop an understanding of the charge transfer and mechanisms of the redox transfer reactions. The surfaces of focus were Li(100), Li_2O, and nanometric Li_2O over Li(100). Other surfaces were studied but did not provide significantly different results. All of these surfaces were optimized with DFT, then annealed with AIMD to 300K in order to create a more accurate picture of the disordered surfaces present experimentally. The bottom layers of these surfaces were fixed during dynamics in order to better represent the bulk material. Li_2S_4 and $(Li_2S_4)_3$ molecules were placed over these surfaces and AIMD was performed, their trajectories were tracked and Bader charge analysis was performed at regular intervals to examine the charge transfer processes. The trimer was used to examine the possibility of surface oxygen being a limiting reactant in the presence of excess sulfide species. All calculations listed were performed at 300K. Additional calculations at 350K, and with an initial velocity placed on the Li_2S_4 species were performed in order to account for the ISL kinetic energy, but no significant differences were observed.

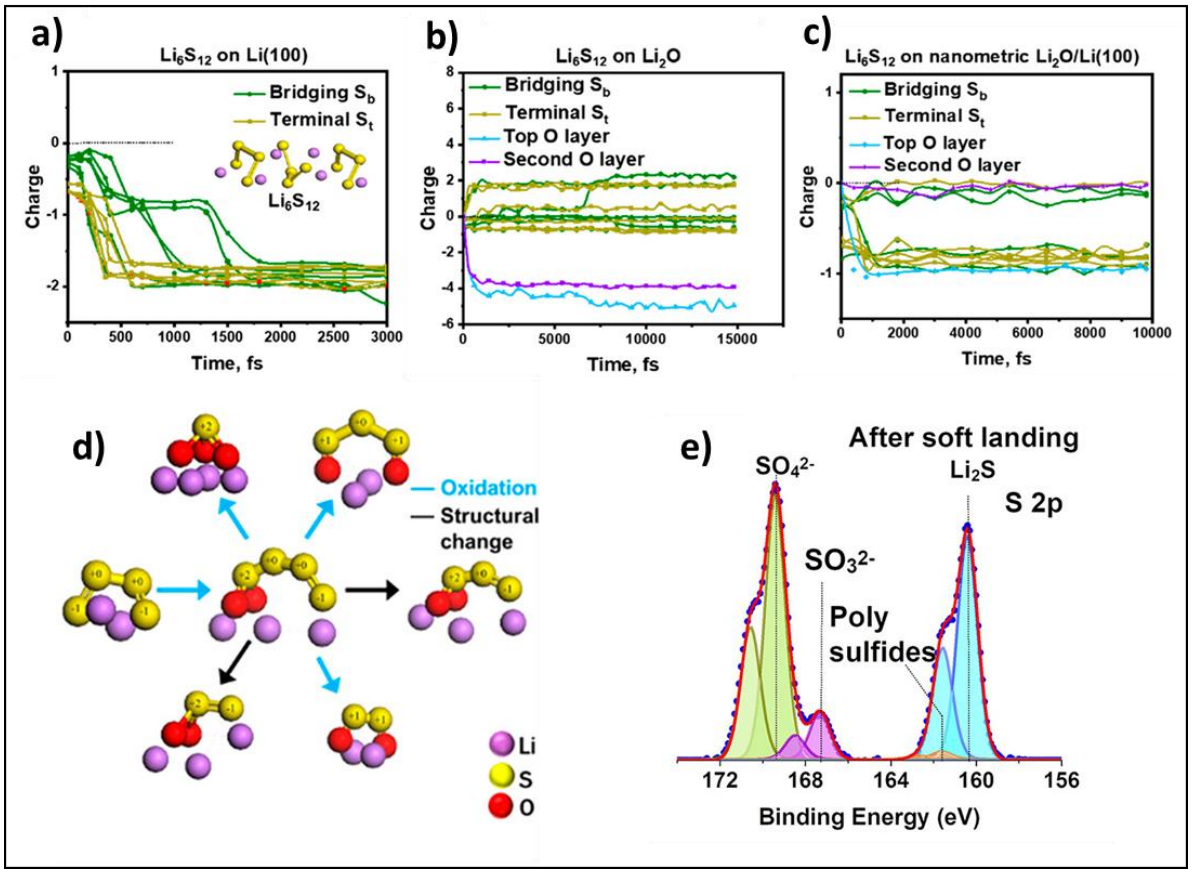

Figure 3: Bader charges of $(Li_2S_4)_3$ on a) Li (100), b) Li_2O, c) nanometric Li2O over Li(100). d) observed reaction pathways of Li_2S_4 on Li_2O. e) XPS spectra of sulfur region after ISL

Reprinted with permission from "Role of Polysulfide Anions in Solid-Electrolyte Interphase Formation at the Lithium Metal Surface in Li–S Batteries"

All polysulfide species on the Li(100) surface rapidly reduced to form the full reduction product Li_2S, with Li_2S_2 as a short-lived intermediate. Bader Charge analysis indicated that these reactions were facilitated by e^- and Li^+ transfer from the surface to the terminal sulfur first, followed by the bridging sulfur. Multiple oxidation products, shown in Figure 3d, were observed for the species deposited on the Li_2O surface. The uppermost oxygen layers in the bulk oxide act as electron acceptors and facilitate the

oxidation of the polysulfide species by an initial step of bonding a terminal sulfur atom to surface oxygen. The species observed here are likely to be metastable products on the pathway to full oxidation, but full oxidation occurs too slowly to observe on the timescale of AIMD. No reactions of the monomer were observed on the nanometric Li_2O layer over Li(100), and only a single reduction was observed for the case of the trimer. This indicates that a thin oxide layer is insulating to reactivity, which can be used to inform future work about designing artificial SEIs to insulate from polysulfide reaction. Significant changes in the coordination and bond lengths of surface Li-O were observed, which further indicated the involvement of the surface in facilizing the polysulfide reaction, and raises questions about the effect of crystal defects that could be explored in future studies.

In summary, in this project we have outlined a methodology for exploring the interfacial reactivity between individual electrolyte species and well-defined electrode surfaces. Our AIMD calculations corroborated the formation of species observed experimentally. We were able to determine the relationship between the surface chemistry of lithium-based substrates and the redox pathways of sulfur species on those surfaces, and outline the mechanisms of those pathways. We were also able to suggest guidance for future studies on the tunability of the SEI and the effect of surface defects on interfacial reactions.

This was a collaborative work with Dr. Balbuena's group at the Texas A&M University Department of Chemical Engineering and Dr. Murugesan's group under JCESR at the Pacific Northwest National Laboratory. Dr. Prabhakaran performed the

ion-soft landing and Mass Spectrometry. Dr. Swadipta, Dr. Shutthanandan, Dr. Wi, and I performed XPS measurements. I performed all of the DFT and AIMD calculations. All authors contributed to the data analysis.

3.4. Reactivity and SEI Formation by TFSI Anions on Lithium Metal Surfaces[§]

This project was designed as a follow-up to the polysulfide work discussed in section 3.3, the data acquisition for this work is complete and we are in the process of writing the manuscript. In this project we followed a similar methodology as the previous work in order to examine the interfacial reactivity of a popular salt in lithium-ion systems, bis(trifluoromethane)sulfonimide ($TFSI^-$). This project is ongoing, all data acquisition is complete, we are currently working on the manuscript and hope to submit it for review in the next 1-2 months.

Lithium foil was sputter-cleaned under ultra-high vacuum conditions and XPS measurements were performed in order to develop baseline data, revealing the presence of LiF, Li_2O, Li_2CO_3, and Li-C groups remaining on the surface. The foil was then transferred *in vacuo* to an ion soft-landing chamber where $TFSI^-$ was deposited onto the surface. The sample was transferred *in vacuo* back to the Fourier Transform infrared spectroscopy (FTIR) and XPS chamber and *in-situ* analysis of the surface was performed.

[§] This is an ongoing project; copyright permissions will be obtained after publication.

FTIR measurements were performed as a function of deposition time. Initial measurements showed the presence of N-O, SO_2, and C=O contaminants. After $TFSI^-$ deposition, C-H, CH3-OH, S_x, SO_2, CF_3, and LiF were observed, indicating that LiF, polysulfide, and ester compounds are common reaction products of $TFSI^-$ with Li metal.

XPS spectra revealed many species on the lithium surface, including Li_2CO_3, CF_3, CF_2, C-N, ester and ether groups, SO_x, and Li_2O. The relative concentrations of species on the surface indicated that the primary reaction products were Li_3N, LiF, S_x, Li_2S_2, and Li_2S.

In order to develop a comparison to previous study, Li foil was placed in a 1M LiTFSI DME solution for 1 hour, after which Raman spectroscopy measurements were performed on the sample. Peaks corresponding to LiOH, Li_2O, Li_2CO_3 and intact $TFSI^-$ were observed, LiF was observed to be the most prevalent reaction product.

The baseline XPS measurements indicated that even after sputter cleaning in pristine conditions, the lithium surface remained a heterogeneous combination of pure metal, oxides, carbonates, and other chemistries. We used DFT and AIMD to study the adsorption behavior and reactivity of LiTFSI over several of these lithium-based surfaces, Li(100), Li_2O, Li_2CO_3, nanometric Li_2O and Li_2CO_3 over Li(100), in order to isolate the experimentally-observed products to their respective surface chemistries.

The relatively-large size and polarity of the TFSI anion suggests that the orientation of the molecule relative to the surface may have an influence on its adsorption and reaction behavior. In order to investigate this, we performed DFT calculations to determine the adsorption energies E_{ads} of four different confirmations of a

LiTFSI molecule over a Li (100) surface: CF_3 groups facing surface, oxygen facing surface, molecule 'side' facing surface, and the molecule in a trans conformation. The respective adsorption energies of these orientations were -0.03eV, -0.5eV, -0.25eV, and -0.06eV. The relatively high E_{ads} of the CF_3-down orientation indicates the least-favorable and most unstable adsorption, and the relatively low value for the O-down orientation indicates the most favorable and stable adsorption. We repeated the calculations of these two orientations for every other surface in this study, the results are shown below in Table 1.

E_{ads} (eV)	**Li (100)**	**Li_2O**	**Li_2CO_3**	**Li_2O/Li(100)**	**Li_2CO_3/Li(100)**
CF_3-down	-0.03	-0.03	+0.01	+0.03	-0.16
O-down	-0.50	-0.02	-0.22	-0.03	-0.01

Table 1. Adsorption energies in eV of TFSI in two orientations over selected surfaces.

We then performed AIMD calculations of both orientations on each surface in order to examine the influence of orientation and surface chemistry on reactivity and reaction products. Both orientations decomposed rapidly (<1ps) over the Li (100) surface. A net 13 electrons was transferred from the surface to the molecule in the CF_3-down orientation. Reaction was initiated by the cleavage of a S-N bond, followed by S-C and 2x S-O cleavage of the same sulfur atom, and complete decomposition of the CF_3 group. The O-down orientation gained a total of 10 electrons from the surface. Interestingly, reaction was initiated by a cleavage of the S-C bond, followed by S-N of the same sulfur, and complete decomposition of the CF_3 group. The final products of

both orientations are similar, with the exception of a fully decomposed vs. stable SO_2 on the surface, which accounts for the difference in net electron transfer. This group decomposes (<1ps) quickly after formation for the CF_3-down orientation, but remains stable for 6ps in the O-down orientation. This difference shows that the less-favorable adsorption creates a more reactive and energetic system that enables reactions that will not occur for species that are more-stably adsorbed. This influences the reaction mechanism, net electron transfer, and final products formed.

The O-down orientation of LiTFSI was observed to be the more favorable adsorption mechanism over the Li_2CO_3 bulk surface. In contrast to the other surfaces, the CF_3-down orientation was the more favorable adsorption mode on the Li_2CO_3/Li(100) surface, this may be because the negatively charged oxygen help stabilize the carbonate surface as it localizes negative charge near the bulk metal interface. AIMD simulations of LiTFSI over the Li_2CO_3 and Li_2CO_3/Li(100) surfaces exhibited no reaction in either orientation. This is seemingly in disagreement with prior study[150], where LiTFSI was observed to react on Li_2CO_3/Li(100) in solution. This suggests that solvent plays a significant role in the reactivity of the molecule. In order to investigate this possibility, we performed additional AIMD calculations of a single DME molecule over the adsorbed LiTFSI in the less-favorable O-down orientation. A 2-electron transfer reaction was observed in this case, by mechanism of a S-C and single C-F cleavage. A surface-bonded CF_2 species remained stable for several ps to the end of the simulation, this species reacts quickly in all other systems, which indicates that this surface may have limited ability to transfer electrons to the fragment. No reaction of the DME molecule

occurred, indicating that the solvent serves as a stabilizing species to enable reaction, without reacting itself.

There was not a significant difference in the adsorption energies of the two orientations over the Li_2O surface, and both modes were relatively unfavorable when compared to values in other systems, which indicates a general instability of LiTFSI over Li_2O. In both cases, a net two electrons were donated from the surface to the molecule, one from the top oxygen layers, and one from the surface lithium. Both of the LiTFSI underwent cis → trans conformational changes before reaction was initiated by S-C bond cleavage. For the CF_3-down orientation, the LiTFSI broke into larger fragments and formed surface-bonded species, including intact CF_3 and SO_2 groups stabilized by surface oxygen. Two of the fragments re-formed through a C-N bond, which was observed in our XPS analysis. In the O-down orientation, the CF_3 fragment fully decomposed and the remainder of the molecule remained intact bonded to the surface. The difference in CF_3 behavior is caused by the surface species that interacts with the group; surface oxygen stabilizes the C-F bonds, but surface Lithium decompose them. It should be noted that even though there is a net transfer of two electrons in each system, some simultaneous reaction steps involve both the acceptance and donation of electrons between the surface and different fragments, and thus there are more than two electrons involved in the overall reaction process.

A similar adsorption behavior is observed for Li_2O/Li(100) systems; the O-down orientation was moderately more favorable, but it exhibits a relatively high E_{ads}. AIMD calculations showed rapid (<1ps) decomposition of the LiTFSI in both orientations over

the bulk Li_2O surface. Both of the orientations reacted occurred more slowly (4-5ps) over the Li_2O/Li(100) surface, this is possibly due to sluggish electron transfer from the bulk lithium metal through the oxide layer. The lithium in the surface donate 3 electrons to the CF_3-down orientation and initiate reaction via S-C cleavage, forming a large surface-bonded fragment and a fully decomposed CF_3. The O-down orientation undergoes reaction similarly to what was observed by Kamphaus et. al[150], where the surface lithium donates 2 electrons to cleave the LiTFSI across the S-N bond and generate two surface-bonded fragments. The behavior of these Li_2O-based systems further corroborates that the initial orientation of the adsorbed species has a strong influence on the reaction pathway and final products.

A wide range of products, including both oxidized and reduced species, were observed during the AIMD calculations, including LiF, Li_2S, LiC, Li_2O, Li_2CO_3, CF_x, sulfites, and other large fragments. All of the observed products, along with Bader charge tracking of selected systems, are shown in Figure 4. With the exception of Li_3N, which likely forms too slowly to observe with AIMD, these products are in good agreement with our experimental observations. CF_3 decomposition to form LiF occurred in almost every system, but there is little other consistency. The nanometric layer systems exhibited lower reactivity and generally larger and fewer decomposition products, likely caused by sluggish electron transfer from the bulk Li through the surface layer.

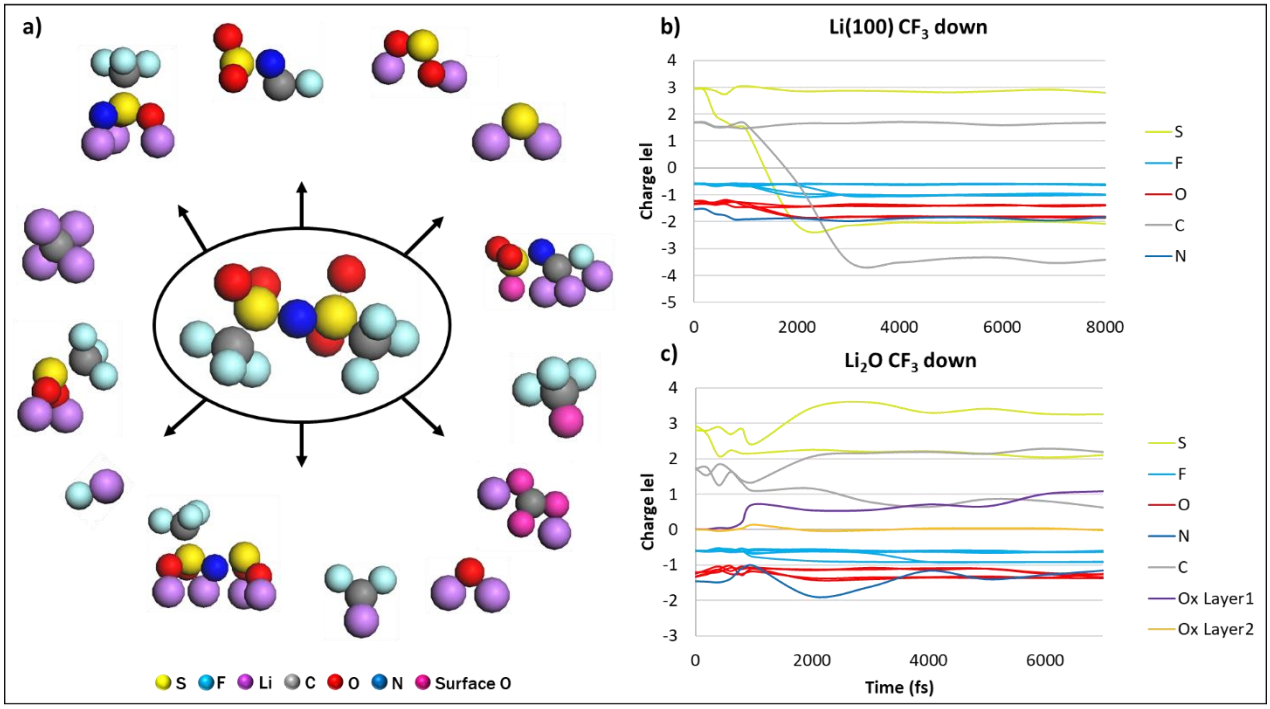

Figure 4. Reaction products observed from LiTFSI decomposition (a). Bader charges of LiTFSI during decomposition over Li (100) (b) and bulk Li_2O (c)

Electronic structure and radial distribution analysis of the Li_2O and Li_2O/Li(100) surfaces revealed significant structural changes before and after LiTFSI decomposition. The peaks of the Li-Li, Li-O, and O-O first coordination shells for the Li_2O surface all became less defined and more spread out after reaction. The coordination shells for the Li_2O/Li(100) surface also become less sharply-defined, but indicate more complex changes than those exhibited by the bulk material. For the CF_3-down orientation, the first Li-Li coordination shell shifts closer together, and the Li-O and O-O shells shift further away. For the O-down orientation, the Li-Li and Li-O shells spread out evenly, and the O-O shell shifts further away. The asymmetrical shifts of these shells in the nanometric

systems indicate larger structural changes occur at the interface as the bulk metal transfers electrons through the oxide.

In summary, this work has developed a detailed understanding of the isolated reactivity of $TFSI^-$ with lithium surfaces. We determined that both the surface chemistry and orientation of the molecule relative to the surface have a significant impact on the reaction pathway and final products. We also determined that solvent species can enable reaction on otherwise-unreactive surfaces. This work provides great insight onto the chemistry of a common salt, and reinforces the efficacy of this combined ISL/XPS/theoretical methodology for isolating and observing pristine chemistries.

This was a collaborative work with Dr. Balbuena's group at the Texas A&M University Department of Chemical Engineering and Dr. Murugesan's group under JCESR at the Pacific Northwest National Laboratory. Dr. Prabhakaran performed the ion-soft landing and Mass Spectrometry. Luke Soule and Dr. Shutthanandan performed XPS measurements. Dr. Prabhakaran and Luke Soule performed FTIR, Raman, and NMR measurements. I performed all of the DFT and AIMD calculations. All authors contributed to the data analysis.

3.5. [**]Combined Density Functional Theory/Kinetic Monte Carlo Investigation of Surface Morphology During Cycling of Li-Cu Electrodes[153]

In this project we employed a combined DFT and KMC approach to investigate the interfacial behavior of nanoporous lithium-copper electrodes. Previous experimental studies have shown promising results of the cycling stability of these systems[46]. We use computational methods to develop an understanding of the atomistic and nanoscale phenomena that influence this promising behavior.

The first portion of this project used DFT in VASP to add lithium atoms one-by-one to copper surfaces with different morphologies; a pristine Cu (111) slab, a slab with a Cu adatom, a slab with a Cu vacancy, and a Cu slab with a nanometric pit. The adsorption energies, E_{ads}, of lithium atoms, shown in Figure 5b, were calculated at each point using the equation:

$$Ea_{ds} = E_{total} - E_{previous} - E_{atom}$$

Where E_{total} is the energy of the system after the atom is adsorbed, $E_{previous}$ is the energy of the previous iteration, and E_{atom} is the energy of the Li atom in the gas phase. The average adsorption energies up to the 25th adsorption in the first 3 systems all had similar values of ~-1.95eV/atom, but the average value for the system with the nanometric pit was -2.4eV, 20% lower than the other systems, which strongly indicates that nanoporous copper facilitates favorable lithium adsorption, and can be used to guide intercalation.

[**] Reprinted with permission from "Combined density functional theory/kinetic Monte Carlo investigation of surface morphology during cycling of Li-Cu electrodes" by K. Hankins, E.P. Kamphaus, P.B. Balbuena, 2021. Electrochimica Acta, 397, Page Range, Copyright 2021 by Elsevier.

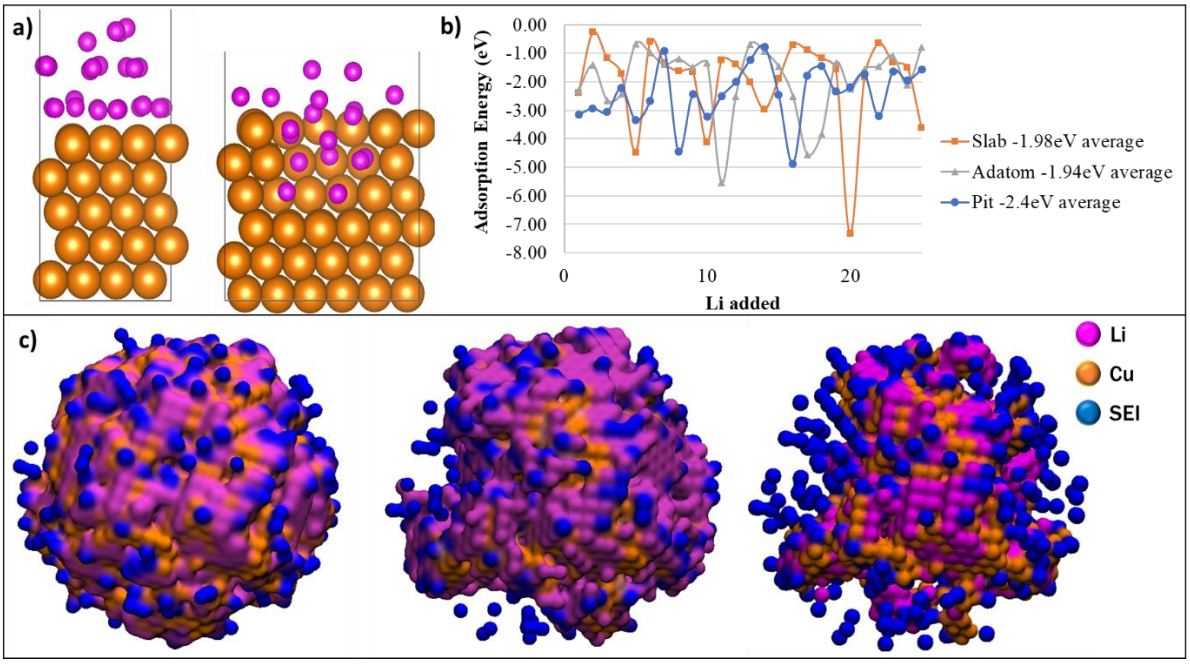

Figure 5: a) DFT Li adsorption on Cu (111) and nanopore. b) Adsorption energies of Li atoms on copper surfaces. c) Evolution of CuLi electrode during KMC charge cycling.

Reprinted with permission from "Combined density functional theory/kinetic Monte Carlo investigation of surface morphology during cycling of Li-Cu electrodes"

We then used DFT and AIMD to develop bonding and reaction parameters for a larger-scale KMC model in order to investigate the stripping/plating behavior lithium on these electrodes during charge cycling. Bonding interactions were obtained using DFT to optimize a bulk crystal and then calculate the single-point energy of the system with (E_{sys}) and without (E_{vac}) a single atom removed. The following equation was used to calculate the bond energy for a given species:

$$E_{bond} = (E_{sys} - E_{vac} - E_{atom})/n_{bonds}$$

Constrained AIMD calculations were used to obtain the energy barrier for a species dissolving from the surface into the electrolyte. This energy was then applied

implicitly in the KMC model in the interactions between the electrolyte and metallic species. The specific details of the KMC code are described in the original manuscript[154], and all reactions were based on a modified Butler-Volmer equation[155]:

$$k_{p,i} = A_{p,i} exp[-\frac{E_{B,i} + \alpha_{p,i}(E - E_{0p,i})}{k_B T}]$$

where

$k_{p,i}$ = rate of reaction p at site i

$A_{p,I}$ = rate prefactor

$E_{B,i}$ = total bonding energy (Energy per bond*number of neighbors)

E = applied potential

$E_{0p,i}$ = standard reduction potential for a species

$\alpha_{p,i}$ = charge transfer coefficient (assumed 0.5 in all cases)

k_B = Boltzmann's constant

T = Temperature (298K for all simulations)

All KMC systems were nanoparticles 27 Å in diameter surrounded by 25 Å of solvent (DME, represented by point masses), five compositions of varying Cu:Li ratio, with a 30% vacancy fraction, were studied, and each was studied with and without the initial presence of a SEI layer, represented by inert species. The initial composition of the clusters was randomly distributed, and each was subjected to an initial diffusion-based equilibration for 20,000 steps before the cycling calculations were performed. During this equilibration, we observed that copper and lithium preferentially formed a segregated nanoalloy rather than remaining homogeneously dispersed, which is in

agreement with prior studies[156], and corroborates the validity of our model. Each system underwent 100 cycles of voltage cycling, where the polarity was switched whenever no more species could dissolve, and recharging was limited to the number of steps in the prior discharge cycle. This implicitly accounts for mass balance of the ions in the system.

The initial composition of the Cu-Li alloy had a significant effect on the behavior of the system. The composition of the cluster changed over time as species were stripped and plated during cycling. Systems with high concentrations of copper remained stable throughout 100 cycles, and acted as effective scaffolds for lithium. Systems with low copper concentrations underwent high amounts of copper stripping due to the clustering behavior of the species; since there was little copper initially, the system could not form stable segregated nanoalloys that retained the copper. The surface area of each system relative to cycle number was studied in order to quantify the morphological changes of the electrode. Systems with high lithium concentrations show initial increases in surface area as fresh lithium preferentially plate onto the surface rather than filling into the electrode pores. This increase in not observed in systems with higher copper concentrations, indicating that copper effectively guides lithium deposition into nanopores. Overall, systems with lower morphological change (high stability) also had lower effective capacities due to the larger presence of copper in the systems, indicating a tradeoff between stability and capacity that could be the subject of further optimization. The surface area in every system eventually decreased due to the

irreversible formation of SEI species, indicating that heterogeneous SEI growth may inhibit the effectiveness of the structured electrode.

We also tracked the capacity of each system using the ratio of Li discharged in a given cycle compared to the total Li in the system. Systems with high lithium fractions underwent substantial capacity losses over 100 cycles, about 60%, with and without the presence of an SEI. Systems with high copper concentrations underwent lower, but still significant, capacity loss, about 45% without an SEI and 10-20% with an SEI. These values indicate that there is a synergistic effect between the presence of the SEI and the copper scaffolding. This observation has inspired a further study that will be discussed in section 3.6. In some systems, dramatic changes to the capacity and surface area were observed during a small cycling window. Further investigation revealed that these changes corresponded to a 'crack' forming in the SEI layer, these cracks exposed the electrode core to the electrolyte and significantly increased the morphological change of the systems. This suggests that a thicker SEI layer may be necessary to effectively protect the core during cycling.

Overall, this project showed promising nanoscale verification of the ability for nanostructured copper electrodes to guide lithium deposition. We documented relationships between the alloy composition and electrode stability and capacity, and observed possible synergistic effects between copper scaffolding and the presence of an SEI, inspiring future studies. Additionally, the KMC model we developed here is robust and has potential to be applied to other applications beyond battery chemistry, including mineral dissolution (Section **A.3**).

This work was performed entirely by Dr. Balbuena's group at the Texas A&M University Department of Chemical Engineering. Dr. Kamphaus performed calculations to obtain reaction prefactors. I performed all other calculations. The KMC code used in this work was adapted from a previous code by a former PhD student from Balbuena's group, Dr. Callejas-Tovar.

3.6. Kinetic Monte Carlo Investigation of SEI Influence on Cycling Behavior of Cu-Li Electrodes[††]

This project is a follow-up to the project discussed in section **3.5**. The findings in the last project raised some interesting questions about the SEI that we seek to investigate here. In this project, we have improved the ability of our KMC model to represent the SEI more explicitly. I am working with and training an undergraduate student on this project, we plan to have the work completed and submitted for review by May of this year.

We have adapted the KMC to represent the SEI more precisely; LiF and Li_2O species are now represented explicitly and can react, rather than in the prior method where they were represented by inert species that only interact to the system through bonding. We have developed interaction parameters for these new species, as well as generated more precise parameters for the species we have used in the past. This project focuses on 24 different systems, consisting of combinations of 2 geometries

[††] This is an ongoing project; copyright permissions will be obtained after publication.

(nanoparticle and periodic slab), 2 electrode chemistries ($Li_{42}Cu_{28}Vac_{30}$, $Li_{28}Cu_{42}Vac_{30}$), 2 SEI chemistries (LiF and Li_2O), and 3 SEI formation rates (reactivity of the electrolyte). Example systems are shown below in Figure 6. In this project, we hope to expand the robustness of our KMC code, and develop a more detailed understanding of the behavior of the SEI and lithium intercalation of nanostructured copper anodes. Some example images from this project are shown below. Please note that these are arbitrary images taken to illustrate the process, not provide data.

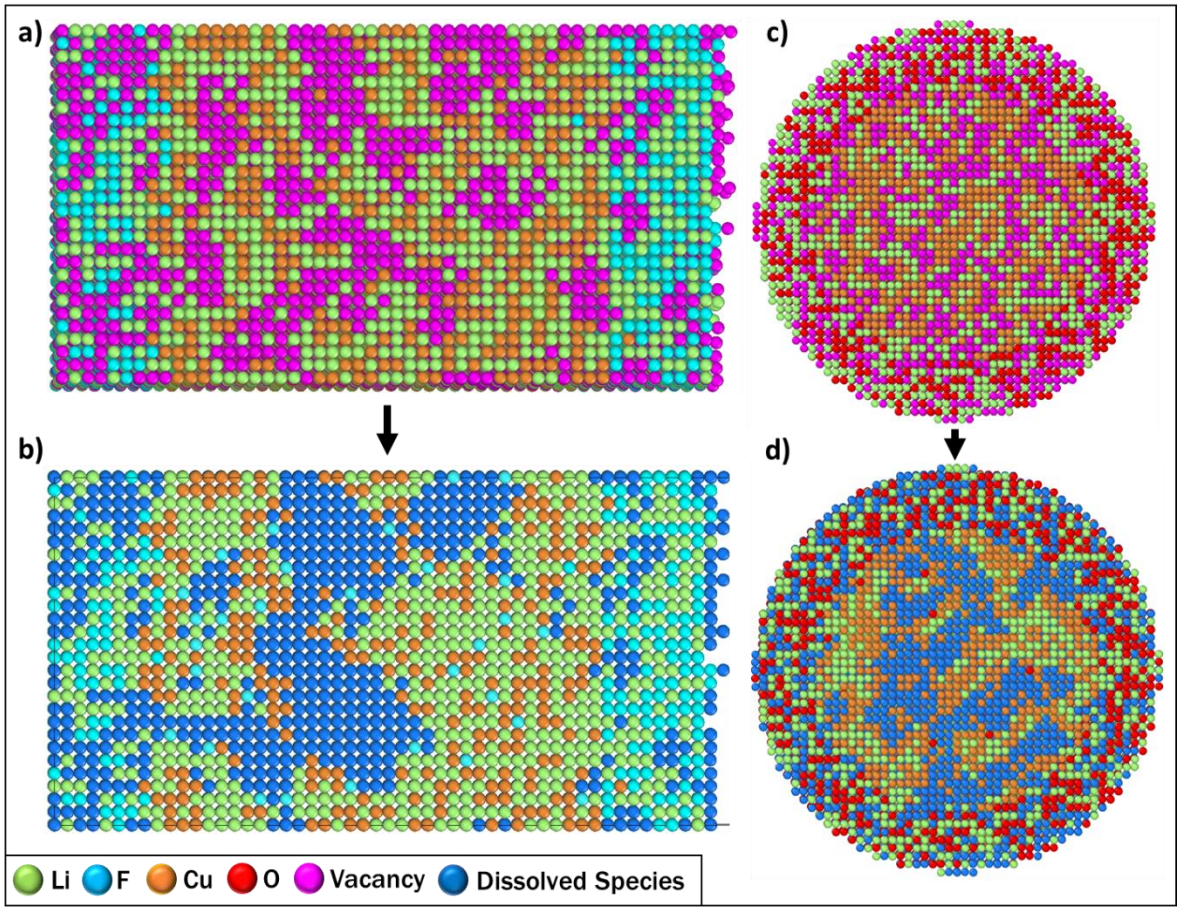

Figure 6. $Li_{0.42}Cu_{0.28}Vac_{0.3}$ slab anode with LiF SEI before (a) and after cycling (b) $Li_{0.28}Cu_{0.42}Vac_{0.3}$ nanoparticle anode with LiO SEI before (c) and after cycling (d)

This work is performed entirely by Dr. Balbuena's group at the Texas A&M University Department of Chemical Engineering. Cameron Kirschvink and I performed all KMC calculations. I performed all DFT calculations and parameterization.

4. SOLVATION PHENOMENA

The projects discussed in this chapter pertain to the solvation behavior of different components in the electrolyte solutions of battery systems. These electrolytic solutions are complex mixtures of solvent(s), salt(s), ion(s), additive(s), and catalyst(s) molecules. The solvation behavior of these systems directly impacts the behavior of the battery through surface reactivity, ion transport, ion solvation and desolvation, and catalytic product transport. Many new complex chemicals and combinations are being explored, some with promising results, but the nanoscale solvation phenomena and underlying mechanisms in these systems are not well understood. We use theoretical methods in order to explore these phenomena.

4.1. ‡‡Phthalocyanine Based Catalyst for Rechargeable Lithium-Oxygen Batteries

In this work, which has been accepted for publication, we use a combined experimental and theoretical approach to examine a Li-Phthalocyanine-based (Li-Pc) catalyst for O_2 transport in lithium-air batteries. Phthalocyanine-based catalysts have shown promising ability to extend cycle life in previous studies, where the molecule acts as a shuttle to reversibly transport O_2^- from the cathode to the insulator deposition surface[157,158]. We observed that the presence of a LiPc catalyst caused significant improvements to the cycle life stability of the Li-oxygen system.

‡‡ This work has been accepted for publication, but is not yet in print yet. The copyright will be updated when it is available.

The experimental cells in this study consisted of a hierarchically porous carbon cathode with a tetraethylene glycol dimethyl ether (TEGDME) solvent with and without a soluble tetrabutylammonium (TBA)-LiPc catalyst. Initial discharge profiles showed a marked improvement in capacity in the system with LiPc 5.28 mAh vs 1.47 mAh without the catalyst, over a 3x increase.

The effect of the catalyst on cycling stability was examined in a pure oxygen with a limited capacity of 0.55mAh. The system with LiPc maintained cycling stability up to 100 cycles (Figure 7a), where it was stopped arbitrarily. This same system without the presence of the catalyst failed after 37 cycles (Figure 7b). An additional cell with catalyst was cycled using air from a dry room (0.01% humidity) as the oxygen source, in which failure occurred after 151 cycles. The presence of LiPc provides a significant improvement to both the capacity and longevity of the Li-air system.

Cyclic voltammetry measurements showed reduction peaks that corresponded to known values of Pc ($Pc \rightarrow Pc^{-1} \rightarrow Pc^{2-}$) and oxygen ($O_2 \rightarrow O_2^{-} \rightarrow O_2^{2-}$) during the forward scan and oxidation peaks that correspond to the reverse processes in the reverse scan. These peaks show that the Pc catalyst is actively participating in the cycling process, and that the typically-detrimental superoxide (O_{2-}) species is present in the system. The stability of the system in spite of the presence of this superoxide species suggests that the LiPc complex successfully reduces and transports O_2, and stably-solvates the superoxide species.

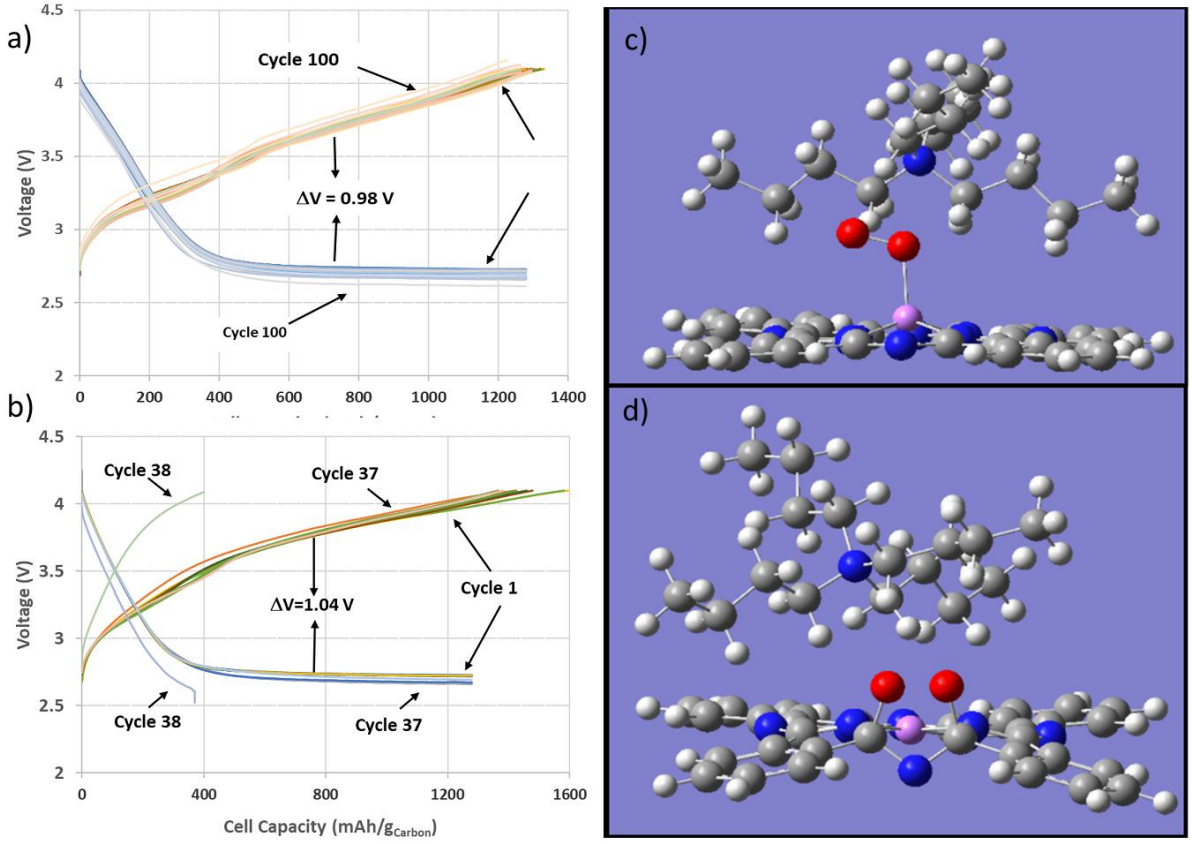

Figure 7: a) Cycling of Li-air cell in oxygen with 2mM TBA-LiPc. b) Cycling of Li-air cell in oxygen without catalyst. c) Geometry of triplet O_2 complexed with TBA-LiPc d) Geometry of singlet O_2 complexed with TBA-LiPc. Carbon are shown in grey, hydrogen in white, oxygen in red, nitrogen in blue, and lithium in pink.

Density functional theory was used in order to develop an understanding of the solvation phenomena and complexation of O_2 with this TBA-LiPc group. These calculations were performed using the Gaussian 16 program with the M05-2X functional (known to simulate dimer species well[159]) and 6-311G(d) basis set. The species of interest were surrounded by the self-consistent reaction field (SCRF) implicit solvent system where the dielectric constant was set to that of TEGDME[160]. Calculations were performed with both a singlet and triplet state forced onto the O_2 species. In the case of

the triplet state, the O-O bond length increased from the gas-phase value of 1.2 Å to 1.32 Å upon complexation, this value corresponds well to the value of the superoxide state. A charge transfer is observed in this case which corresponds to Pc acting as a catalyst for oxygen reduction. The singlet O_2, recognized as the main source of decomposition in Li-air systems, reacted with the Pc anion to form an out-of-plane 5-membered ring. This reaction is similar to products that have been observed in previous studies[161], and possibly explains the source of these products. The singlet oxygen system was 0.05eV less stable than the triplet, this low barrier suggests that system can easily switch between the two states during transport. The ability of this LiPc catalyst to trap singlet oxygen may explain the long cycle life observed experimentally; the singlet oxygen is trapped in the complex and is unable to induce electrolyte decomposition.

This work illustrated the effectiveness of the TBA-LiPc catalyst in increasing the capacity and cycle life of lithium-air systems. Higher capacities and longer cycle lives were observed in systems with the presence of catalyst relative to without. DFT calculations showed that the TBA-LiPc complex can readily trap singlet and triplet oxygen and suggest that this complex is responsible for the overall effectiveness of the system.

This was a collaborative work with the Dr. Scanlon's group at the U.S. Air Force Research Laboratory, Dr. Feld's group at the Wright State University Department of Chemistry, and Dr. Balbuena's group at the Texas A&M University Department of Chemical Engineering. I performed all theoretical calculations. Dr. Scanlon supervised

battery fabrication and measurements. Dr. Feld performed synthesis and characterization of the systems.

4.2. Solvation Behavior of Mg^{2+} Ions in Ternary Electrolyte with Molecular PTO Cathode[§§]

In this currently-ongoing project, we employ theoretical methods in order to investigate the solvation and desolvation phenomena and clustering of a promising new electrolyte system proposed by Dong *et al*[48]. We are using CMD calculations to study the solvation behavior of Mg - monocarborane - dimethoxyethane - bis(2-methoxyethyl) ether (abbreviated as MMC-DME-G2) electrolyte solution in the presence of an organic molecular cathode: pyrene-4,5,9,10-tetraone (PTO). This system proposed by Dong *et al* improves the kinetics of the Mg battery system in two ways. First, it circumvents the normally-sluggish Mg^{2+} reduction process by harnessing the enolization chemistry of the PTO molecule to enable fast reduction kinetics at the cathode. And second, it employs a weakly-coordinating salt, MMC, in a DME/G2 solvent that is less viscous and less strongly-coordinating than normal solvents like G4; which enables rapid ion transport through the bulk electrolyte and faster ion desolvation at the cathode. This system exhibited promising behavior experimentally, but the ion solvation/desolvation and transport mechanisms of this novel cathode and electrolyte are not well-understood. In this project, we are using theoretical methods in order to develop an understanding of

[§§] This is an ongoing project; copyright permissions will be obtained after publication.

these mechanisms in order to inform the tuning of future cathode and electrolyte chemistries based on this system.

The monocarborane anion used in this system is a relatively novel species, and no atomic force fields for it were available in literature. We performed DFT calculations with the Gaussian 16 program in order to develop novel OPLS-aa force field parameters for the monocarborane anion. We first performed geometry optimizations and obtained atomic charges using the CHELPG method[162] with the mp2 functional and 6-311g(d) basis set[162,163]. We then used the scan method in Gaussian with a mp2 functional and 6-31g(d) basis set to stretch the angles and bonds in the molecule in order to obtain the harmonic constants for CMD simulations[164]. These parameters were verified by performing CMD calculations and comparing the calculated density (~1.11 g/cm^3) to our experimental values (1.11-1.17g/cm^3). All other species in our CMD calculations used the standard OPLS-aa force fields[165], we repeated the CHELPG calculations on the PTO molecules in order to determine specific atomic charges for each molecular charge state.

We performed CMD simulations for 40nanoseconds of the electrolyte solution described in the experimental work (0.5mol/kg MMC in 1:1 wt% DME/G2), in order to examine the coordination complexes that form. We repeated this for several cases: with and without the presence of PTO, three charge states for PTO (-0. -2, and -4), excess MMC salt (0.88mol/kg), and with an excess of PTO. The excess systems were studied in order to examine if larger-scale clustering of the species could occur. Radial distribution functions were used to develop a quantitative understanding of the coordination behavior, some of these functions are shown in Figure 8. Coordination numbers

correspond to the number of sites coordinated at 3.5Å, coordinate-contact ion pair percentage is defined by the percent of sites within 3Å of the species relative to the total amount within 8Å of the species.

In every system, we observed a similar amount of DME and G2 coordinated to Mg^{2+}, indicating that neither species preferentially solvates the ion over the other. All systems showed a Mg-MC contact ion pair percentage of less than 12% compared to solvent-separated pairing, indicating that MC^- successfully acts as a weakly coordinating anion. Visual examination of the trajectories showed a wide array (over 20) of different solvation complexes for magnesium, which indicates that there is not a particular complex structure that is significantly more favorable.

Magnesium coordination to DME and G2 decreased in every system as the charge of PTO decreased. Mg-MC coordination decreased with decreasing PTO charge except in the systems with excess MMC, where it increased. Mg-PTO coordination increased as PTO was reduced from the neutral to -2 charge state, but decreased when it was further reduced to the -4 charge state. The coordinate contact pair % of all species followed the trends of the overall coordination in every system; when coordination decreases, the species that still remain coordinated do so at a further distance. These trends show that reduced PTO will pull cations away from the solvent species, they also indicate that PTO^{-2} will accept the first cation more readily than PTO^{4-} will accept the second cation. This implies that this is an effective system to enable Mg^{2+} intercalation into the cathode.

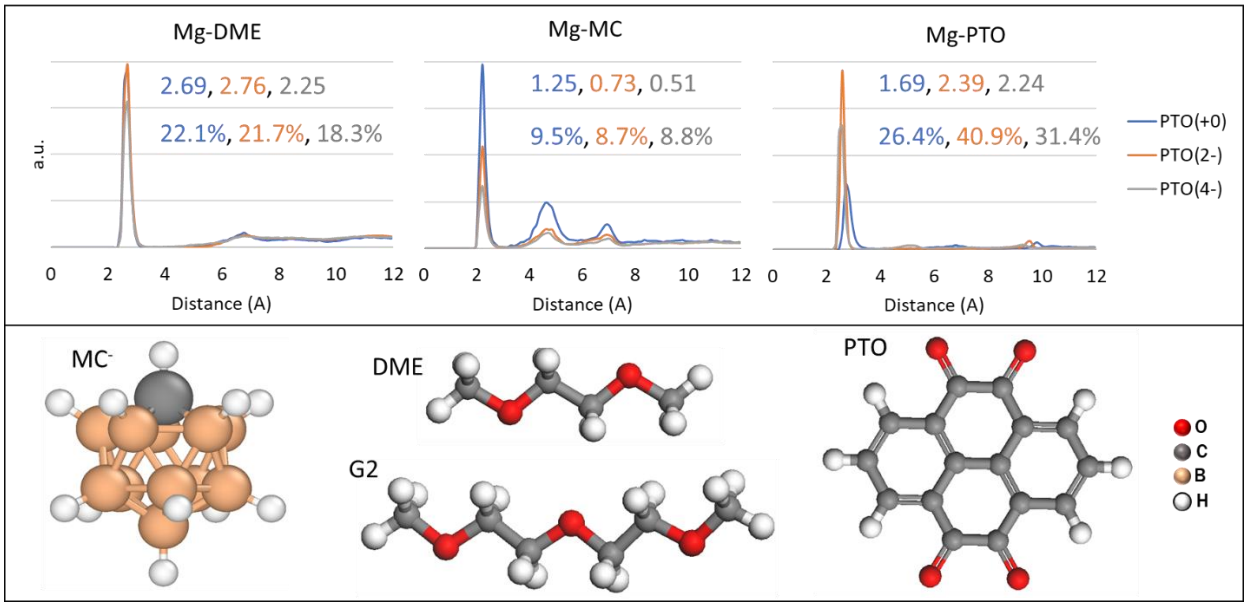

Figure 8. Top: Selected RDF graphs from systems with standard compositions. Raw numbers indicate the site coordination number for that system, percentages indicate the percent of coordinate contact ion pairs for the corresponding species in the given system. Bottom: Species studied in these simulations.

The systems with excess MMC and excess PTO showed significantly increased self-coordination of the excess species, indicating that clustering is possible in these conditions, and may become more pronounced at larger timescales.

Additional CMD calculations were performed on these systems with an electric field applied to the cations in order to encourage dynamics. Three different ionic transport modes were observed in these calculations. The first involves the cation moving rapidly through the electrolyte with little coordination to any species, this occurs in high fields and active systems. The second mode involves the cation strongly coordinating to the electrolyte species, and the entire complex moving through the bulk, this occurs at low electric fields, and is likely representative of what may happen in the bulk electrolyte, far from the electrode. The last transport mechanism is by-far the most

common, and consists of the cation temporarily coordinating to several species, and then being 'handed off' to new species, forming a new temporary complex, this occurs in all system conditions. An example image of this mechanism is shown below in Figure 9. This is likely enabled by the weakly-coordinating electrolyte species, and could explain the rapid ionic transport observed experimentally; the cation is not trapped by slow-moving viscous complexes.

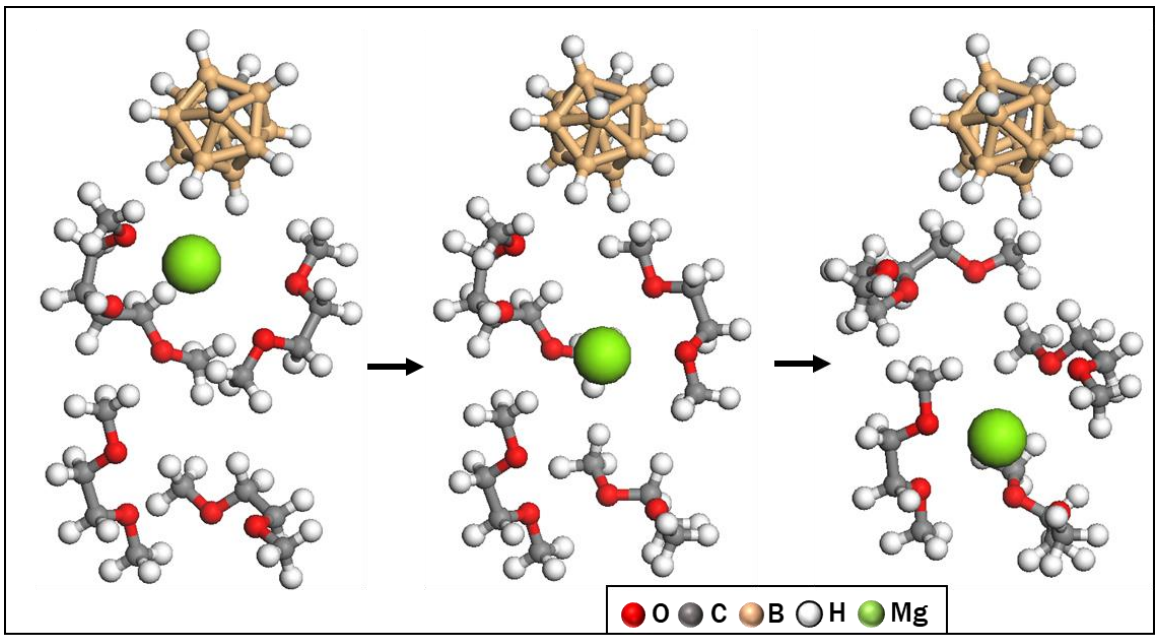

Figure 9: Example of third Mg^{2+} transport mode, where the ion is initially solvated by MC-G2-DME, and is handed off to form a MG-3DME complex. Please note that this is an example image artificially generated in order to illustrate the concept.

We plan to perform additional applied-field CMD calculations in the future to study the ion solvation/desolvation behavior of the PTO cathode. These calculations, coupled with the ones that are completed, should provide a clear picture of the solvation behavior of this system.

This is a collaborative work with Dr. Yao's group at the University of Houston Department of Electrical and Computer Engineering, Dr. Rana Mohtadi from Toyota, and Dr. Balbuena's group at the Texas A&M University Department of Chemical Engineering.

5. CONCLUSIONS

In this section I will summarize the motivations for my research and the projects I have discussed above. I will conclude this dissertation with a discussion of my future career and research pathways.

5.1. Summary

The environmental dangers posed by greenhouse gas-induced climate change has created a global demand to more towards renewable energy resources. Current energy storage technology cannot meet the demands of a full shift towards renewable energy; more robust and sustainable battery technology is required to meet the energy storage needs of the future. Many new battery technologies are being investigated to meet these demands, but they face significant challenges in stability and durability. These challenges are induced by a number of phenomena related to the surface reactivity and morphology of the electrodes, and ion solvation and transport in the electrolyte.

In my research, I use computational methods to explore the nanoscale mechanisms and behavior that drives these phenomena. My work can be divided into two main branches: surface reactivity and morphology, and solvation phenomena. I have worked with many different battery chemistries and configurations in collaboration with several experimental and theoretical groups in order to develop a nanoscale understanding of behavior that is observed on a larger scale.

The reactions and morphological changes that occur at electrode surfaces play a significant role in battery function; they can both make the battery more stable, and cause catastrophic failure. I have investigated these phenomena in different ways; by

developing a fundamental mechanistic understanding of their behavior, by studying the effect of specific chemistries on SEI formation, and by understanding the mechanisms that enable promising solutions to their negative effects.

My projects discussed in sections 3.1 and 3.2 seek to develop an understanding of the mechanisms behind the phenomena that influence surface reactivity and morphology. The work in section 3.1 developed a model of the initial stages of SEI growth and structure for two common SEI components. The study in section 3.2 developed a nanoscale understanding of the expansion-induced failure of silicon electrodes and SEI coatings.

The projects discussed in sections 3.3 and 3.4 seek to develop a clear picture of the reaction behavior of specific chemical species over lithium surfaces. The work in section 3.3 outlined a novel method for precisely examining battery surface chemistry, and provided insight on the behavior of polysulfide reactivity and tunability for Li-S batteries. The project outlined in section 3.4 will extend this methodology onto a common electrolyte, LiTFSI, in order to develop a better understanding of the chemistry behind SEI formation. Future work can extend this methodology to new species to develop a more widespread understanding of their individual reaction behavior.

The projects discussed in sections 3.2, 3.5, and 3.6, seek to understand the nanoscale phenomena that enable effective solutions towards stable and reversible lithium intercalation. The second portion of the project in section 3.2 examined the adhesive properties and reaction behavior of surface coatings that have been proposed as a way to mitigate failure in Li-Si batteries. The work discussed in section 3.5 sought to

develop an effective KMC model for battery simulation, and to outline the nanoscale phenomena that enable stable lithium intercalation in a promising new nanostructured electrode. The project outlined in section 3.6 extends the prior project to better-represent the SEI and understand the relationship between the SEI and this nanostructured electrode. The KMC model developed here can be extended to many other battery chemistries and formulations in order to develop a better overall understanding of cycling behavior.

The solvation phenomena and ionic transport behavior through the electrolyte determine the rate of charge and discharge in the battery, and can heavily influence the surface behaviors mentioned in the prior paragraph. My projects over solvation phenomena seek to understand the complex mechanisms that enable promising new chemistries to readily transport ions and species in challenging systems, in order to inform the selections of future chemistries.

The project discussed in section 4.1 explores the use of a new catalytic species that enables more effective and stable cycling in Li-air batteries. We were able to confirm the effectiveness of this species, and show on the atom-scale that the catalyst will readily transport oxygen. Future work will examine more detailed transport properties with this catalyst complex, and examine new electrolyte chemistries.

My project discussed in section 4.2 seeks to understand the complex phenomena that enable the stable cycling of a new Mg-based battery system. I have developed novel modeling parameters and developed an understanding of the solvent coordination and ionic transport in this system. This project will continue by developing an understanding

of the ion solvation/desolvation phenomena with the novel cathode material. This will provide a detailed understanding of the system that can be used to tune future chemistries.

Battery function is controlled by a wide range of interconnected phenomena from the electrode surfaces and electrolyte. My research seeks to further the overall understanding of these behaviors in order to help develop new battery chemistries that can meet the substantial energy storage requirements of the future.

Future studies should work in two main modes: The first should work to develop a precise and detailed understanding of individual chemistries and surfaces in order to help delineate the specific interactions in these complex systems. The second should work to acknowledge the interconnectedness of all of these phenomena, and to study how this interconnectedness changes the overall behavior relative to the individual parts. This process would develop a broad understanding of battery and surface chemistry that can be used to guide the selection and tuning of new systems and chemistries.

5.2. Future Plans

I plan to graduate in May of 2022 and pursue a career in computational research with a focus on batteries and interfacial chemistry. I have accepted a post-doctoral position working under Dr. Ulrike Krewer in the Post-Lithium-Storage (PoLiS) cluster at the Karlsruhe Institute of Technology in Karlsruhe, Germany. I will be working to develop a generalized KMC model for battery systems with a focus on the behavior of the SEI. This position is expected to last 1-2 years, during which they will provide

opportunities for me to learn how to manage a research group if I am interested. I do not know the specific career path that I wish to follow after this position, but I hope to follow a path in either private or public research that lets me use scientific principles to improve energy storage and change the world.

REFERENCES

(1) John Pethica; Fiona Fox; Brian Hoskins; Michael Kelly. Climate Change: A Summary of the Science. *The Royal Society* **2010**.

(2) Abnett, K. Shift to Renewable Energy Eases Key Environmental Burdens, EU Says. *Reuters*. 2021.

(3) Pinson, P.; Mitridati, L.; Ordoudis, C.; Østergaard, J. Towards Fully Renewable Energy Systems: Experience and Trends in Denmark. *CSEE Journal of Power and Energy Systems* **2017**, *3* (1), 26–35. https://doi.org/10.17775/CSEEJPES.2017.0005.

(4) Owusu, P. A.; Asumadu-Sarkodie, S. A Review of Renewable Energy Sources, Sustainability Issues and Climate Change Mitigation. *Cogent Engineering* **2016**, *3* (1), 1167990. https://doi.org/10.1080/23311916.2016.1167990.

(5) Dunn, B.; Kamath, H.; Tarascon, J.-M. Electrical Energy Storage for the Grid: A Battery of Choices. *Science* **2011**, *334* (6058), 928–935.

(6) Manz, D.; Piwko, R.; Miller, N. Look Before You Leap: The Role of Energy Storage in the Grid. *IEEE Power and Energy Magazine* **2012**, *10* (4), 75–84. https://doi.org/10.1109/MPE.2012.2196337.

(7) Hesse, H. C.; Schimpe, M.; Kucevic, D.; Jossen, A. Lithium-Ion Battery Storage for the Grid—A Review of Stationary Battery Storage System Design Tailored for Applications in Modern Power Grids. *Energies* **2017**, *10* (12), 2107.

(8) Puranen, P.; Kosonen, A.; Ahola, J. Technical Feasibility Evaluation of a Solar PV Based Off-Grid Domestic Energy System with Battery and Hydrogen Energy Storage in Northern Climates. *Solar Energy* **2021**, *213*, 246–259. https://doi.org/10.1016/j.solener.2020.10.089.

(9) Fotouhi, A.; Auger, D. J.; Propp, K.; Longo, S.; Wild, M. A Review on Electric Vehicle Battery Modelling: From Lithium-Ion toward Lithium–Sulphur. *Renewable and Sustainable Energy Reviews* **2016**, *56*, 1008–1021. https://doi.org/10.1016/j.rser.2015.12.009.

(10) Young, K.; Wang, C.; Wang, L. Y.; Strunz, K. Electric Vehicle Battery Technologies. In *Electric Vehicle Integration into Modern Power Networks*; Garcia-Valle, R., Peças Lopes, J. A., Eds.; Power Electronics and Power Systems; Springer: New York, NY, 2013; pp 15–56. https://doi.org/10.1007/978-1-4614-0134-6_2.

(11) Yoshino, A. The Birth of the Lithium-Ion Battery. *Angewandte Chemie International Edition* **2012**, *51* (24), 5798–5800. https://doi.org/10.1002/anie.201105006.

(12) Scrosati, B. Recent Advances in Lithium Ion Battery Materials. *Electrochimica Acta* **2000**, *45* (15), 2461–2466. https://doi.org/10.1016/S0013-4686(00)00333-9.

(13) Chen, M.; Wang, R.; Qi, Y.; Han, Y.; Wang, R.; Fu, J.; Meng, F.; Yi, X.; Huang, J.; Shu, J. Cobalt and Lithium Leaching from Waste Lithium Ion Batteries by Glycine. *Journal of Power Sources* **2021**, *482*, 228942. https://doi.org/10.1016/j.jpowsour.2020.228942.

(14) Boyden, A.; Soo, V. K.; Doolan, M. The Environmental Impacts of Recycling Portable Lithium-Ion Batteries. *Procedia CIRP* **2016**, *48*, 188–193. https://doi.org/10.1016/j.procir.2016.03.100.

(15) Sovacool, B. K. The Precarious Political Economy of Cobalt: Balancing Prosperity, Poverty, and Brutality in Artisanal and Industrial Mining in the Democratic Republic of the Congo. *The Extractive Industries and Society* **2019**, *6* (3), 915–939. https://doi.org/10.1016/j.exis.2019.05.018.

(16) Li, M.; Lu, J. Cobalt in Lithium-Ion Batteries. *Science* **2020**, *367* (6481), 979–980. https://doi.org/10.1126/science.aba9168.

(17) Liu, B.; Zhang, J.-G.; Xu, W. Advancing Lithium Metal Batteries. *Joule* **2018**, *2* (5), 833–845. https://doi.org/10.1016/j.joule.2018.03.008.

(18) Manthiram, A. An Outlook on Lithium Ion Battery Technology. *ACS Cent. Sci.* **2017**, *3* (10), 1063–1069. https://doi.org/10.1021/acscentsci.7b00288.

(19) Chen, S.; Zheng, J.; Mei, D.; Han, K. S.; Engelhard, M. H.; Zhao, W.; Xu, W.; Liu, J.; Zhang, J.-G. High-Voltage Lithium-Metal Batteries Enabled by Localized High-Concentration Electrolytes. *Advanced Materials* **2018**, *30* (21), 1706102. https://doi.org/10.1002/adma.201706102.

(20) Ji, B.; Zhang, F.; Song, X.; Tang, Y. A Novel Potassium-Ion-Based Dual-Ion Battery. *Advanced Materials* **2017**, *29* (19), 1700519. https://doi.org/10.1002/adma.201700519.

(21) Araujo, R. B.; Thangavel, V.; Johansson, P. Towards Novel Calcium Battery Electrolytes by Efficient Computational Screening. *Energy Storage Materials* **2021**, *39*, 89–95. https://doi.org/10.1016/j.ensm.2021.04.015.

(22) Song, J.; Sahadeo, E.; Noked, M.; Lee, S. B. Mapping the Challenges of Magnesium Battery. *J. Phys. Chem. Lett.* **2016**, *7* (9), 1736–1749. https://doi.org/10.1021/acs.jpclett.6b00384.

(23) Challenges and Prospects of Lithium–Sulfur Batteries | Accounts of Chemical Research https://pubs.acs.org/doi/abs/10.1021/ar300179v (accessed 2021 -04 -19).

(24) Xiuxia Zuo; Jin Zhu; Peter Müller-Buschbaum; Ya-Jun Cheng. Silicon Based Lithium-Ion Battery Anodes: A Chronicle Perspective Review. *Nano Energy* **2017**, *31*, 113–143.

(25) Shin, H.-C.; Liu, M. Three-Dimensional Porous Copper–Tin Alloy Electrodes for Rechargeable Lithium Batteries. *Advanced Functional Materials* **2005**, *15* (4), 582–586. https://doi.org/10.1002/adfm.200305165.

(26) Balbuena, P. B.; Wang, Y. X. *Lithium-Ion Batteries: Solid-Electrolyte Interphase*; World Scientific, 2004.

(27) Heiskanen, S. K.; Kim, J.; Lucht, B. L. Generation and Evolution of the Solid Electrolyte Interphase of Lithium-Ion Batteries. *Joule* **2019**, *3* (10), 2322–2333. https://doi.org/10.1016/j.joule.2019.08.018.

(28) Verma, P.; Maire, P.; Novák, P. A Review of the Features and Analyses of the Solid Electrolyte Interphase in Li-Ion Batteries. *Electrochimica Acta* **2010**, *55* (22), 6332–6341. https://doi.org/10.1016/j.electacta.2010.05.072.

(29) Gao, Y.; Du, X.; Hou, Z.; Shen, X.; Mai, Y.-W.; Tarascon, J.-M.; Zhang, B. Unraveling the Mechanical Origin of Stable Solid Electrolyte Interphase. *Joule* **2021**, *5* (7), 1860–1872. https://doi.org/10.1016/j.joule.2021.05.015.

(30) Jurng, S.; L. Brown, Z.; Kim, J.; L. Lucht, B. Effect of Electrolyte on the Nanostructure of the Solid Electrolyte Interphase (SEI) and Performance of Lithium Metal Anodes. *Energy & Environmental Science* **2018**, *11* (9), 2600–2608. https://doi.org/10.1039/C8EE00364E.

(31) Li, F.; He, J.; Liu, J.; Wu, M.; Hou, Y.; Wang, H.; Qi, S.; Liu, Q.; Hu, J.; Ma, J. Gradient Solid Electrolyte Interphase and Lithium-Ion Solvation Regulated by Bisfluoroacetamide for Stable Lithium Metal Batteries. *Angewandte Chemie International Edition* **2021**, *60* (12), 6600–6608. https://doi.org/10.1002/anie.202013993.

(32) Saha, P.; Datta, M. K.; Velikokhatnyi, O. I.; Manivannan, A.; Alman, D.; Kumta, P. N. Rechargeable Magnesium Battery: Current Status and Key Challenges for

the Future. *Progress in Materials Science* **2014**, *66*, 1–86. https://doi.org/10.1016/j.pmatsci.2014.04.001.

(33) Gao, T.; Hou, S.; Huynh, K.; Wang, F.; Eidson, N.; Fan, X.; Han, F.; Luo, C.; Mao, M.; Li, X.; Wang, C. Existence of Solid Electrolyte Interphase in Mg Batteries: Mg/S Chemistry as an Example. *ACS Appl. Mater. Interfaces* **2018**, *10* (17), 14767–14776. https://doi.org/10.1021/acsami.8b02425.

(34) Bae, J.; Park, H.; Guo, X.; Zhang, X.; H. Warner, J.; Yu, G. High-Performance Magnesium Metal Batteries via Switching the Passivation Film into a Solid Electrolyte Interphase. *Energy & Environmental Science* **2021**, *14* (8), 4391–4399. https://doi.org/10.1039/D1EE00614B.

(35) Song, W.; Stein Scholtis, E.; C. Sherrell, P.; H. Tsang, D. K.; Ngiam, J.; Lischner, J.; Fearn, S.; Bemmer, V.; Mattevi, C.; Klein, N.; Xie, F.; Jason Riley, D. Electronic Structure Influences on the Formation of the Solid Electrolyte Interphase. *Energy & Environmental Science* **2020**, *13* (12), 4977–4989. https://doi.org/10.1039/D0EE01825B.

(36) Wang, C.; Wu, H.; Chen, Z.; McDowell, M. T.; Cui, Y.; Bao, Z. Self-Healing Chemistry Enables the Stable Operation of Silicon Microparticle Anodes for High-Energy Lithium-Ion Batteries. *Nature Chemistry* **2013**, *5* (12), 1042–1048. https://doi.org/10.1038/nchem.1802.

(37) González, S. I.; Oña, O. B.; Ferraro, M. B.; Facelli, J. C. Structure and Electronic Properties of Lithium–Silicon Clusters. *Computational and Theoretical Chemistry* **2013**, *1024*, 61–68.

(38) Li, W.; Yao, H.; Yan, K.; Zheng, G.; Liang, Z.; Chiang, Y.-M.; Cui, Y. The Synergetic Effect of Lithium Polysulfide and Lithium Nitrate to Prevent Lithium Dendrite Growth. *Nature communications* **2015**, *6* (1), 1–8.

(39) Matyjaszewski, K.; Tsarevsky, N. V. Nanostructured Functional Materials Prepared by Atom Transfer Radical Polymerization. *Nature Chem* **2009**, *1* (4), 276–288. https://doi.org/10.1038/nchem.257.

(40) Luo, J.; Fang, C.-C.; Wu, N.-L. High Polarity Poly(Vinylidene Difluoride) Thin Coating for Dendrite-Free and High-Performance Lithium Metal Anodes. *Advanced Energy Materials* **2018**, *8* (2), 1701482. https://doi.org/10.1002/aenm.201701482.

(41) Liu, W.; Li, W.; Zhuo, D.; Zheng, G.; Lu, Z.; Liu, K.; Cui, Y. Core–Shell Nanoparticle Coating as an Interfacial Layer for Dendrite-Free Lithium Metal Anodes. *ACS Cent. Sci.* **2017**, *3* (2), 135–140. https://doi.org/10.1021/acscentsci.6b00389.

(42) Wei, L.; Chen, C.; Hou, Z.; Wei, H. Poly (Acrylic Acid Sodium) Grafted Carboxymethyl Cellulose as a High Performance Polymer Binder for Silicon Anode in Lithium Ion Batteries. *Sci Rep* **2016**, *6* (1), 19583. https://doi.org/10.1038/srep19583.

(43) Luo, W.; Chen, X.; Xia, Y.; Chen, M.; Wang, L.; Wang, Q.; Li, W.; Yang, J. Surface and Interface Engineering of Silicon-Based Anode Materials for Lithium-Ion Batteries. *Advanced Energy Materials* **2017**, *7* (24), 1701083. https://doi.org/10.1002/aenm.201701083.

(44) Xiao, Z.; Lei, C.; Yu, C.; Chen, X.; Zhu, Z.; Jiang, H.; Wei, F. Si@Si3N4@C Composite with Egg-like Structure as High-Performance Anode Material for Lithium Ion Batteries. *Energy Storage Materials* **2020**, *24*, 565–573. https://doi.org/10.1016/j.ensm.2019.06.031.

(45) Zhao, H.; Lei, D.; He, Y.-B.; Yuan, Y.; Yun, Q.; Ni, B.; Lv, W.; Li, B.; Yang, Q.-H.; Kang, F.; Lu, J. Compact 3D Copper with Uniform Porous Structure Derived by Electrochemical Dealloying as Dendrite-Free Lithium Metal Anode Current Collector. *Advanced Energy Materials* **2018**, *8* (19), 1800266. https://doi.org/10.1002/aenm.201800266.

(46) Cao, Z.; Li, B.; Yang, S. Dendrite-Free Lithium Anodes with Ultra-Deep Stripping and Plating Properties Based on Vertically Oriented Lithium–Copper–Lithium Arrays. *Advanced Materials* **2019**, *31* (29), 1901310. https://doi.org/10.1002/adma.201901310.

(47) Zhang, R.; Li, N.-W.; Cheng, X.-B.; Yin, Y.-X.; Zhang, Q.; Guo, Y.-G. Advanced Micro/Nanostructures for Lithium Metal Anodes. *Advanced Science* **2017**, *4* (3), 1600445. https://doi.org/10.1002/advs.201600445.

(48) Dong, H.; Tutusaus, O.; Liang, Y.; Zhang, Y.; Lebens-Higgins, Z.; Yang, W.; Mohtadi, R.; Yao, Y. High-Power Mg Batteries Enabled by Heterogeneous Enolization Redox Chemistry and Weakly Coordinating Electrolytes. *Nature Energy* **2020**, *5* (12), 1043–1050. https://doi.org/10.1038/s41560-020-00734-0.

(49) Shao, Y.; Liu, T.; Li, G.; Gu, M.; Nie, Z.; Engelhard, M.; Xiao, J.; Lv, D.; Wang, C.; Zhang, J.-G.; Liu, J. Coordination Chemistry in Magnesium Battery Electrolytes: How Ligands Affect Their Performance. *Scientific Reports* **2013**, *3* (1), 3130. https://doi.org/10.1038/srep03130.

(50) Girishkumar, G.; McCloskey, B.; Luntz, A. C.; Swanson, S.; Wilcke, W. Lithium−Air Battery: Promise and Challenges. *J. Phys. Chem. Lett.* **2010**, *1* (14), 2193–2203. https://doi.org/10.1021/jz1005384.

(51) Grande, L.; Paillard, E.; Hassoun, J.; Park, J.-B.; Lee, Y.-J.; Sun, Y.-K.; Passerini, S.; Scrosati, B. The Lithium/Air Battery: Still an Emerging System or a Practical Reality? *Advanced Materials* **2015**, *27* (5), 784–800. https://doi.org/10.1002/adma.201403064.

(52) Wang, Y.; Lu, Y.-R.; Dong, C.-L.; Lu, Y.-C. Critical Factors Controlling Superoxide Reactions in Lithium–Oxygen Batteries. *ACS Energy Lett.* **2020**, *5* (5), 1355–1363. https://doi.org/10.1021/acsenergylett.0c00365.

(53) Torres, W. R.; Davia, F.; Pozo, M. del; Tesio, A. Y.; Calvo, E. J. EQCM and RDE/RRDE Study of Soluble Iron Phthalocyanine Bifunctional Catalyst for the Lithium-Oxygen Battery. *J. Electrochem. Soc.* **2017**, *164* (14), A3785. https://doi.org/10.1149/2.1441714jes.

(54) Runge, E.; Gross, E. K. U. Density-Functional Theory for Time-Dependent Systems. *Phys. Rev. Lett.* **1984**, *52* (12), 997–1000. https://doi.org/10.1103/PhysRevLett.52.997.

(55) Mardirossian, N.; Head-Gordon, M. Thirty Years of Density Functional Theory in Computational Chemistry: An Overview and Extensive Assessment of 200 Density Functionals. *Molecular Physics* **2017**, *115* (19), 2315–2372. https://doi.org/10.1080/00268976.2017.1333644.

(56) Kohn, W.; Sham, L. J. Self-Consistent Equations Including Exchange and Correlation Effects. *Phys. Rev.* **1965**, *140* (4A), A1133–A1138. https://doi.org/10.1103/PhysRev.140.A1133.

(57) Born, M.; Oppenheimer, R. Zur Quantentheorie Der Molekeln. *Annalen der Physik* **1927**, *389* (20), 457–484. https://doi.org/10.1002/andp.19273892002.

(58) Pisana, S.; Lazzeri, M.; Casiraghi, C.; Novoselov, K. S.; Geim, A. K.; Ferrari, A. C.; Mauri, F. Breakdown of the Adiabatic Born–Oppenheimer Approximation in Graphene. *Nature Mater* **2007**, *6* (3), 198–201. https://doi.org/10.1038/nmat1846.

(59) Burke, K. Perspective on Density Functional Theory. *J. Chem. Phys.* **2012**, *136* (15), 150901. https://doi.org/10.1063/1.4704546.

(60) Challenges for Density Functional Theory | Chemical Reviews https://pubs.acs.org/doi/full/10.1021/cr200107z (accessed 2021 -11 -24).

(61) Cohen, A. J.; Mori-Sánchez, P.; Yang, W. Insights into Current Limitations of Density Functional Theory. *Science* **2008**, *321* (5890), 792–794. https://doi.org/10.1126/science.1158722.

(62) Verma, P.; Truhlar, D. G. Status and Challenges of Density Functional Theory. *Trends in Chemistry* **2020**, *2* (4), 302–318. https://doi.org/10.1016/j.trechm.2020.02.005.

(63) Stephan Kümmel; Leeor Kronik. Orbital-Dependent Density Functionals: Theory and Applications. *The Journal of Chemical Physics* **2008**, *80* (1). https://doi.org/10.1103/RevModPhys.80.3.

(64) Marom, N.; Tkatchenko, A.; Rossi, M.; Gobre, V. V.; Hod, O.; Scheffler, M.; Kronik, L. Dispersion Interactions with Density-Functional Theory: Benchmarking Semiempirical and Interatomic Pairwise Corrected Density Functionals. *J. Chem. Theory Comput.* **2011**, *7* (12), 3944–3951. https://doi.org/10.1021/ct2005616.

(65) Boese, A. D.; Martin, J. M. L.; Handy, N. C. The Role of the Basis Set: Assessing Density Functional Theory. *The Journal of Chemical Physics* **2003**, *119* (6), 3005–3014. https://doi.org/10.1063/1.1589004.

(66) Pople, J. A.; Gill, P. M. W.; Johnson, B. G. Kohn—Sham Density-Functional Theory within a Finite Basis Set. *Chemical Physics Letters* **1992**, *199* (6), 557–560. https://doi.org/10.1016/0009-2614(92)85009-Y.

(67) Hehre, W. J.; Stewart, R. F.; Pople, J. A. Self-Consistent Molecular-Orbital Methods. I. Use of Gaussian Expansions of Slater-Type Atomic Orbitals. *J. Chem. Phys.* **1969**, *51* (6), 2657–2664. https://doi.org/10.1063/1.1672392.

(68) Ditchfield, R.; Hehre, W. J.; Pople, J. A. Self-Consistent Molecular-Orbital Methods. IX. An Extended Gaussian-Type Basis for Molecular-Orbital Studies of Organic Molecules. *J. Chem. Phys.* **1971**, *54* (2), 724–728. https://doi.org/10.1063/1.1674902.

(69) Lehtola, S.; Blockhuys, F.; Van Alsenoy, C. An Overview of Self-Consistent Field Calculations Within Finite Basis Sets. *Molecules* **2020**, *25* (5), 1218. https://doi.org/10.3390/molecules25051218.

(70) Chong *, D. P. Augmenting Basis Set for Time-Dependent Density Functional Theory Calculation of Excitation Energies: Slater-Type Orbitals for Hydrogen to Krypton. *Molecular Physics* **2005**, *103* (6–8), 749–761. https://doi.org/10.1080/00268970412331333618.

(71) Förster, A.; Visscher, L. Double Hybrid DFT Calculations with Slater Type Orbitals. *Journal of Computational Chemistry* **2020**, *41* (18), 1660–1684. https://doi.org/10.1002/jcc.26209.

(72) Dunlap, B. I.; Rosch, N. The Gaussian-Type Orbitals Density-Functional Approach to Finite Systems. In *Advances in Quantum Chemistry*; Löwdin, P.-O., Ed.; Density Functional Theory of Many-Fermion Systems; Academic Press, 1990; Vol. 21, pp 317–339. https://doi.org/10.1016/S0065-3276(08)60603-6.

(73) Daga, L. E.; Civalleri, B.; Maschio, L. Gaussian Basis Sets for Crystalline Solids: All-Purpose Basis Set Libraries vs System-Specific Optimizations. *J. Chem. Theory Comput.* **2020**, *16* (4), 2192–2201. https://doi.org/10.1021/acs.jctc.9b01004.

(74) M. J. Frisch; G. W. Trucks; H. B. Schlegel; et al. *Gaussian*; Gaussian, Inc.: Wallingford CT, 2016.

(75) E.J. Baerends; T. Ziegler; A.J. Atkins; et. al. *Amsterdam Density Functional*; SCM, Theoretical Chemistry: Vrije Universiteit, Amsterdam, 2019.

(76) te Velde, G.; Bickelhaupt, F. M.; Baerends, E. J.; Fonseca Guerra, C.; van Gisbergen, S. J. A.; Snijders, J. G.; Ziegler, T. Chemistry with ADF. *Journal of Computational Chemistry* **2001**, *22* (9), 931–967. https://doi.org/10.1002/jcc.1056.

(77) Mulliken, R. S. Molecular Compounds and Their Spectra. II. *J. Am. Chem. Soc.* **1952**, *74* (3), 811–824. https://doi.org/10.1021/ja01123a067.

(78) Fonseca Guerra, C.; Handgraaf, J.-W.; Baerends, E. J.; Bickelhaupt, F. M. Voronoi Deformation Density (VDD) Charges: Assessment of the Mulliken, Bader, Hirshfeld, Weinhold, and VDD Methods for Charge Analysis. *Journal of Computational Chemistry* **2004**, *25* (2), 189–210. https://doi.org/10.1002/jcc.10351.

(79) Heine, V. The Pseudopotential Concept. In *Solid State Physics*; Ehrenreich, H., Seitz, F., Turnbull, D., Eds.; Academic Press, 1970; Vol. 24, pp 1–36. https://doi.org/10.1016/S0081-1947(08)60069-7.

(80) Kresse, G.; Joubert, D. From Ultrasoft Pseudopotentials to the Projector Augmented-Wave Method. *Phys. Rev. B* **1999**, *59* (3), 1758–1775. https://doi.org/10.1103/PhysRevB.59.1758.

(81) Makov, G.; Shah, R.; Payne, M. C. Periodic Boundary Conditions in *Ab Initio* Calculations. II. Brillouin-Zone Sampling for Aperiodic Systems. *Phys. Rev. B* **1996**, *53* (23), 15513–15517. https://doi.org/10.1103/PhysRevB.53.15513.

(82) Hafner, J.; Kresse, G. The Vienna AB-Initio Simulation Program VASP: An Efficient and Versatile Tool for Studying the Structural, Dynamic, and Electronic Properties of Materials. In *Properties of Complex Inorganic Solids*;

Gonis, A., Meike, A., Turchi, P. E. A., Eds.; Springer US: Boston, MA, 1997; pp 69–82. https://doi.org/10.1007/978-1-4615-5943-6_10.

(83) Bader, R. F. W.; Henneker, W. H.; Cade, P. E. Molecular Charge Distributions and Chemical Binding. *The Journal of Chemical Physics* **1967**, *46* (9), 3341–3363. https://doi.org/10.1063/1.1841222.

(84) Tang, W.; Sanville, E.; Henkelman, G. A Grid-Based Bader Analysis Algorithm without Lattice Bias. *J. Phys.: Condens. Matter* **2009**, *21* (8), 084204. https://doi.org/10.1088/0953-8984/21/8/084204.

(85) Perdew, J. P.; Burke, K.; Ernzerhof, M. Generalized Gradient Approximation Made Simple. *Phys. Rev. Lett.* **1996**, *77* (18), 3865–3868. https://doi.org/10.1103/PhysRevLett.77.3865.

(86) Heyd, J.; Scuseria, G. E.; Ernzerhof, M. Hybrid Functionals Based on a Screened Coulomb Potential. *J. Chem. Phys.* **2003**, *118* (18), 8207–8215. https://doi.org/10.1063/1.1564060.

(87) Joachim Paier; Martijn Marsman; Georg Kresse. Why Does the B3LYP Hybrid Functional Fail for Metals? *The Journal of Chemical Physics* **2007**, *127* (2). https://doi.org/10.1063/1.2747249.

(88) Kresse, G.; Furthmüller, J. Efficient Iterative Schemes for Ab Initio Total-Energy Calculations Using a Plane-Wave Basis Set. *Phys. Rev. B* **1996**, *54* (16), 11169–11186. https://doi.org/10.1103/PhysRevB.54.11169.

(89) Troullier, N.; Martins, J. L. Efficient Pseudopotentials for Plane-Wave Calculations. *Phys. Rev. B* **1991**, *43* (3), 1993–2006. https://doi.org/10.1103/PhysRevB.43.1993.

(90) Kresse, G.; Hafner, J. Ab Initio Molecular Dynamics for Liquid Metals. *Phys. Rev. B* **1993**, *47* (1), 558–561. https://doi.org/10.1103/PhysRevB.47.558.

(91) Marx, D.; Hutter, J. Ab Initio Molecular Dynamics: Theory and Implementation. *Modern methods and algorithms of quantum chemistry* **2000**, *1* (301–449), 141.

(92) Evans, D. J.; Holian, B. L. The Nose–Hoover Thermostat. *J. Chem. Phys.* **1985**, *83* (8), 4069–4074. https://doi.org/10.1063/1.449071.

(93) Grimme, S.; Antony, J.; Ehrlich, S.; Krieg, H. A Consistent and Accurate Ab Initio Parametrization of Density Functional Dispersion Correction (DFT-D) for the 94 Elements H-Pu. *J. Chem. Phys.* **2010**, *132* (15), 154104. https://doi.org/10.1063/1.3382344.

(94) Alder, B. J.; Wainwright, T. E. Studies in Molecular Dynamics. I. General Method. *The Journal of Chemical Physics* **1959**, *31* (2), 459–466. https://doi.org/10.1063/1.1730376.

(95) Nosé, S. A Unified Formulation of the Constant Temperature Molecular Dynamics Methods. *The Journal of Chemical Physics* **1984**, *81* (1), 511–519. https://doi.org/10.1063/1.447334.

(96) Parrinello, M.; Rahman, A. Polymorphic Transitions in Single Crystals: A New Molecular Dynamics Method. *Journal of Applied Physics* **1981**, *52* (12), 7182–7190. https://doi.org/10.1063/1.328693.

(97) Toukan, K.; Rahman, A. Molecular-Dynamics Study of Atomic Motions in Water. *Phys. Rev. B* **1985**, *31* (5), 2643–2648. https://doi.org/10.1103/PhysRevB.31.2643.

(98) Sutmann, G. Classical Molecular Dynamics. *Quantum simulations of complex many-body systems: from theory to algorithms* **2002**, *10*, 211–254.

(99) Monticelli, L.; Tieleman, D. P. Force Fields for Classical Molecular Dynamics. In *Biomolecular Simulations: Methods and Protocols*; Monticelli, L., Salonen, E., Eds.; Methods in Molecular Biology; Humana Press: Totowa, NJ, 2013; pp 197–213. https://doi.org/10.1007/978-1-62703-017-5_8.

(100) Thompson, A. P.; Aktulga, H. M.; Berger, R.; Bolintineanu, D. S.; Brown, W. M.; Crozier, P. S.; in 't Veld, P. J.; Kohlmeyer, A.; Moore, S. G.; Nguyen, T. D.; Shan, R.; Stevens, M. J.; Tranchida, J.; Trott, C.; Plimpton, S. J. LAMMPS - a Flexible Simulation Tool for Particle-Based Materials Modeling at the Atomic, Meso, and Continuum Scales. *Computer Physics Communications* **2022**, *271*, 108171. https://doi.org/10.1016/j.cpc.2021.108171.

(101) James, F. Monte Carlo Theory and Practice. *Rep. Prog. Phy* **1980**, No. 43.

(102) Metropolis, N.; Ulam, S. The Monte Carlo Method. *Journal of the American Statistical Association* **1949**, *44* (247), 335–341. https://doi.org/10.1080/01621459.1949.10483310.

(103) Cai, Z.; Lu, J. A Quantum Kinetic Monte Carlo Method for Quantum Many-Body Spin Dynamics. *SIAM J. Sci. Comput.* **2018**, *40* (3), B706–B722. https://doi.org/10.1137/17M1145446.

(104) Jansen, A. P. J. *An Introduction to Kinetic Monte Carlo Simulations of Surface Reactions*; Springer, 2012; Vol. 856.

(105) Voter, A. F. Introduction to the Kinetic Monte Carlo Method. In *Radiation effects in solids*; Springer, 2007; pp 1–23.

(106) Battaile, C. C. The Kinetic Monte Carlo Method: Foundation, Implementation, and Application. *Computer Methods in Applied Mechanics and Engineering* **2008**, *197* (41), 3386–3398. https://doi.org/10.1016/j.cma.2008.03.010.

(107) Serebrinsky, S. A. Physical Time Scale in Kinetic Monte Carlo Simulations of Continuous-Time Markov Chains. *Phys. Rev. E* **2011**, *83* (3), 037701. https://doi.org/10.1103/PhysRevE.83.037701.

(108) *Biovia Materials Studio*; Dassault Systèmes: San Diego, 2017.

(109) Jain, A.; Ong, S. P.; Hautier, G.; Chen, W.; Richards, W. D.; Dacek, S.; Cholia, S.; Gunter, D.; Skinner, D.; Ceder, G.; Persson, K. A. Commentary: The Materials Project: A Materials Genome Approach to Accelerating Materials Innovation. *APL Materials* **2013**, *1* (1), 011002. https://doi.org/10.1063/1.4812323.

(110) Martínez, L.; Andrade, R.; Birgin, E. G.; Martínez, J. M. PACKMOL: A Package for Building Initial Configurations for Molecular Dynamics Simulations. *J Comput Chem* **2009**, *30* (13), 2157–2164. https://doi.org/10.1002/jcc.21224.

(111) Jewett, A. I.; Stelter, D.; Lambert, J.; Saladi, S. M.; Roscioni, O. M.; Ricci, M.; Autin, L.; Maritan, M.; Bashusqeh, S. M.; Keyes, T.; Dame, R. T.; Shea, J.-E.; Jensen, G. J.; Goodsell, D. S. Moltemplate: A Tool for Coarse-Grained Modeling of Complex Biological Matter and Soft Condensed Matter Physics. *Journal of Molecular Biology* **2021**, *433* (11), 166841. https://doi.org/10.1016/j.jmb.2021.166841.

(112) Stukowski, A. Visualization and Analysis of Atomistic Simulation Data with OVITO–the Open Visualization Tool. *Modelling Simul. Mater. Sci. Eng.* **2009**, *18* (1), 015012. https://doi.org/10.1088/0965-0393/18/1/015012.

(113) Momma, K.; Izumi, F. VESTA 3 for Three-Dimensional Visualization of Crystal, Volumetric and Morphology Data. *J Appl Cryst* **2011**, *44* (6), 1272–1276. https://doi.org/10.1107/S0021889811038970.

(114) Humphrey, W.; Dalke, A.; Schulten, K. VMD: Visual Molecular Dynamics. *Journal of Molecular Graphics* **1996**, *14* (1), 33–38. https://doi.org/10.1016/0263-7855(96)00018-5.

(115) Fairley, N.; Fernandez, V.; Richard-Plouet, M.; Guillot-Deudon, C.; Walton, J.; Smith, E.; Flahaut, D.; Greiner, M.; Biesinger, M.; Tougaard, S.; Morgan, D.;

Baltrusaitis, J. Systematic and Collaborative Approach to Problem Solving Using X-Ray Photoelectron Spectroscopy. *Applied Surface Science Advances* **2021**, *5*, 100112. https://doi.org/10.1016/j.apsadv.2021.100112.

(116) *Microsoft Excel*; Microsoft Corporation, 2018.

(117) *Origin*; OriginLab Corporation: Northampton, MA, USA.

(118) Chastain, J.; King Jr, R. C. Handbook of X-Ray Photoelectron Spectroscopy. *Perkin-Elmer Corporation* **1992**, *40*, 221.

(119) Charles S.Fadley. Angle-Resolved x-Ray Photoelectron Spectroscopy. *Progress in Surface Science* **1984**, *16* (3). https://doi.org/10.1016/0079-6816(84)90001-7.

(120) *CasaXPS*; Casa Software Ltd., 2019.

(121) NIST X-ray Photoelectron Spectroscopy (XPS) Database https://srdata.nist.gov/xps/main_search_menu.aspx (accessed 2021 -12 -03).

(122) Marzouk, A.; Ponce, V.; Benitez, L.; Soto, F. A.; Hankins, K.; Seminario, J. M.; Balbuena, P. B.; El-Mellouhi, F. Unveiling the First Nucleation and Growth Steps of Inorganic Solid Electrolyte Interphase Components. *J. Phys. Chem. C* **2018**, *122* (45), 25858–25868. https://doi.org/10.1021/acs.jpcc.8b08398.

(123) Lei Fan; Houlong L. Zhuang; Lina Gao; Yingying Lu; Lynden A. Archer. Regulating Li Deposition at Artificial Solid Electrolyte Interphases. *Journal of Materials Chemistry A* **2017**, *6*, 3483–3492. https://doi.org/10.1039/C6TA10204B.

(124) Ponce, V.; Galvez-Aranda, D. E.; Seminario, J. M. Analysis of a Li-Ion Nanobattery with Graphite Anode Using Molecular Dynamics Simulations. *J. Phys. Chem. C* **2017**, *121* (23), 12959–12971. https://doi.org/10.1021/acs.jpcc.7b04190.

(125) Guan, P.; Liu, L.; Lin, X. Simulation and Experiment on Solid Electrolyte Interphase (SEI) Morphology Evolution and Lithium-Ion Diffusion. *J. Electrochem. Soc.* **2015**, *162* (9), A1798. https://doi.org/10.1149/2.0521509jes.

(126) Jieyun Zheng; Hao Zheng; Rui Wang; Liubin Ben; Wei Lu; Liwei Chen; Liquan Chen; Hong Li. 3D Visualization of Inhomogeneous Multi-Layered Structure and Young's Modulus of the Solid Electrolyte Interphase (SEI) on Silicon Anodes for Lithium. *Physical Chemistry Chemical Physics* **2014**, *16*, 13229–13238. https://doi.org/10.1039/C4CP01968G.

(127) Glass, C. W.; Oganov, A. R.; Hansen, N. USPEX—Evolutionary Crystal Structure Prediction. *Computer physics communications* **2006**, *175* (11–12), 713–720.

(128) Oganov, A. R.; Glass, C. W. Crystal Structure Prediction Using Ab Initio Evolutionary Techniques: Principles and Applications. *The Journal of chemical physics* **2006**, *124* (24), 244704.

(129) Heyd, J.; Scuseria, G. E. Efficient Hybrid Density Functional Calculations in Solids: Assessment of the Heyd–Scuseria–Ernzerhof Screened Coulomb Hybrid Functional. *J. Chem. Phys.* **2004**, *121* (3), 1187–1192. https://doi.org/10.1063/1.1760074.

(130) Dovesi, R.; Pascale, F.; Civalleri, B.; Doll, K.; Harrison, N. M.; Bush, I.; D'Arco, P.; Noël, Y.; Rérat, M.; Carbonnière, P.; Causà, M.; Salustro, S.; Lacivita, V.; Kirtman, B.; Ferrari, A. M.; Gentile, F. S.; Baima, J.; Ferrero, M.; Demichelis, R.; De La Pierre, M. The CRYSTAL Code, 1976–2020 and beyond, a Long Story. *J. Chem. Phys.* **2020**, *152* (20), 204111. https://doi.org/10.1063/5.0004892.

(131) Becke, A. D. Density-functional Thermochemistry. III. The Role of Exact Exchange. *J. Chem. Phys.* **1993**, *98* (7), 5648–5652. https://doi.org/10.1063/1.464913.

(132) Doll, K.; Schön, J. C.; Jansen, M. Ab Initio Energy Landscape of LiF Clusters. *J. Chem. Phys.* **2010**, *133* (2), 024107. https://doi.org/10.1063/1.3455708.

(133) Zhang, J.; Wang, R.; Yang, X.; Lu, W.; Wu, X.; Wang, X.; Li, H.; Chen, L. Direct Observation of Inhomogeneous Solid Electrolyte Interphase on MnO Anode with Atomic Force Microscopy and Spectroscopy. *Nano Lett.* **2012**, *12* (4), 2153–2157. https://doi.org/10.1021/nl300570d.

(134) Galvez-Aranda, D. E.; Verma, A.; Hankins, K.; Seminario, J. M.; Mukherjee, P. P.; Balbuena, P. B. Chemical and Mechanical Degradation and Mitigation Strategies for Si Anodes. *Journal of Power Sources* **2019**, *419*, 208–218. https://doi.org/10.1016/j.jpowsour.2019.02.054.

(135) Boukamp, B. A.; Lesh, G. C.; Huggins, R. A. All-Solid Lithium Electrodes with Mixed-Conductor Matrix. *J. Electrochem. Soc.* **1981**, *128* (4), 725–729. https://doi.org/10.1149/1.2127495.

(136) Beaulieu, L. Y.; Eberman, K. W.; Turner, R. L.; Krause, L. J.; Dahn, J. R. Colossal Reversible Volume Changes in Lithium Alloys. *Electrochem. Solid-State Lett.* **2001**, *4* (9), A137. https://doi.org/10.1149/1.1388178.

(137) Kaliaperumal, M.; Dharanendrakumar, M. S.; Prasanna, S.; Abhishek, K. V.; Chidambaram, R. K.; Adams, S.; Zaghib, K.; Reddy, M. V. Cause and Mitigation of Lithium-Ion Battery Failure—A Review. *Materials* **2021**, *14* (19), 5676. https://doi.org/10.3390/ma14195676.

(138) Lyu, D.; Ren, B.; Li, S. Failure Modes and Mechanisms for Rechargeable Lithium-Based Batteries: A State-of-the-Art Review. *Acta Mech* **2019**, *230* (3), 701–727. https://doi.org/10.1007/s00707-018-2327-8.

(139) Chan, C. K.; Peng, H.; Liu, G.; McIlwrath, K.; Zhang, X. F.; Huggins, R. A.; Cui, Y. High-Performance Lithium Battery Anodes Using Silicon Nanowires. *Nature Nanotech* **2008**, *3* (1), 31–35. https://doi.org/10.1038/nnano.2007.411.

(140) Jia, H.; Li, X.; Song, J.; Zhang, X.; Luo, L.; He, Y.; Li, B.; Cai, Y.; Hu, S.; Xiao, X.; Wang, C.; Rosso, K. M.; Yi, R.; Patel, R.; Zhang, J.-G. Hierarchical Porous Silicon Structures with Extraordinary Mechanical Strength as High-Performance Lithium-Ion Battery Anodes. *Nat Commun* **2020**, *11* (1), 1474. https://doi.org/10.1038/s41467-020-15217-9.

(141) Chen, H.; Wu, Z.; Su, Z.; Chen, S.; Yan, C.; Al-Mamun, M.; Tang, Y.; Zhang, S. A Mechanically Robust Self-Healing Binder for Silicon Anode in Lithium Ion Batteries. *Nano Energy* **2021**, *81*, 105654. https://doi.org/10.1016/j.nanoen.2020.105654.

(142) Verma, A.; Mukherjee, P. P. Mechanistic Analysis of Mechano-Electrochemical Interaction in Silicon Electrodes with Surface Film. *J. Electrochem. Soc.* **2017**, *164* (14), A3570. https://doi.org/10.1149/2.0391714jes.

(143) Chen, C.-F.; Barai, P.; Smith, K.; Mukherjee, P. P. Scaling Relations for Intercalation Induced Damage in Electrodes. *Electrochimica Acta* **2016**, *204*, 31–49. https://doi.org/10.1016/j.electacta.2016.03.106.

(144) Barai, P.; Mukherjee, P. P. Stochastic Analysis of Diffusion Induced Damage in Lithium-Ion Battery Electrodes. *J. Electrochem. Soc.* **2013**, *160* (6), A955. https://doi.org/10.1149/2.132306jes.

(145) Galvez-Aranda, D. E.; Seminario, J. M. Simulations of a LiF Solid Electrolyte Interphase Cracking on Silicon Anodes Using Molecular Dynamics. *J. Electrochem. Soc.* **2018**, *165* (3), A717. https://doi.org/10.1149/2.0991803jes.

(146) Hankins, K.; Soto, F. A.; Balbuena, P. B. Insights into the Li Intercalation and SEI Formation on LiSi Nanoclusters. *J. Electrochem. Soc.* **2017**, *164* (11), E3457–E3464. https://doi.org/10.1149/2.0311711jes.

(147) Hankins, K.; Prabhakaran, V.; Wi, S.; Shutthanandan, V.; Johnson, G. E.; Roy, S.; Wang, H.; Shao, Y.; Thevuthasan, S.; Balbuena, P. B.; Mueller, K. T.; Murugesan, V. Role of Polysulfide Anions in Solid-Electrolyte Interphase Formation at the Lithium Metal Surface in Li–S Batteries. *J. Phys. Chem. Lett.* **2021**, *12* (38), 9360–9367. https://doi.org/10.1021/acs.jpclett.1c01930.

(148) Seh, Z. W.; Sun, Y.; Zhang, Q.; Cui, Y. Designing High-Energy Lithium–Sulfur Batteries. *Chem. Soc. Rev.* **2016**, *45* (20), 5605–5634. https://doi.org/10.1039/C5CS00410A.

(149) Pang, Q.; Kundu, D.; Cuisinier, M.; Nazar, L. F. Surface-Enhanced Redox Chemistry of Polysulphides on a Metallic and Polar Host for Lithium-Sulphur Batteries. *Nat Commun* **2014**, *5* (1), 4759. https://doi.org/10.1038/ncomms5759.

(150) Kamphaus, E. P.; Angarita-Gomez, S.; Qin, X.; Shao, M.; Engelhard, M.; Mueller, K. T.; Murugesan, V.; Balbuena, P. B. Role of Inorganic Surface Layer on Solid Electrolyte Interphase Evolution at Li-Metal Anodes. *ACS applied materials & interfaces* **2019**, *11* (34), 31467–31476.

(151) D. Gunaratne, K. D.; Prabhakaran, V.; M. Ibrahim, Y.; V. Norheim, R.; E. Johnson, G.; Laskin, J. Design and Performance of a High-Flux Electrospray Ionization Source for Ion Soft Landing. *Analyst* **2015**, *140* (9), 2957–2963. https://doi.org/10.1039/C5AN00220F.

(152) Liang, X.; Hart, C.; Pang, Q.; Garsuch, A.; Weiss, T.; Nazar, L. F. A Highly Efficient Polysulfide Mediator for Lithium–Sulfur Batteries. *Nat Commun* **2015**, *6* (1), 5682. https://doi.org/10.1038/ncomms6682.

(153) K.Hankins; E.P.Kamphaus; P.B.Balbuena. Combined Density Functional Theory/Kinetic Monte Carlo Investigation of Surface Morphology during Cycling of Li-Cu Electrodes. *Electrochimica Acta* **2021**, *397*. https://doi.org/10.1016/j.electacta.2021.139272.

(154) Callejas-Tovar, R.; Diaz, C. A.; de la Hoz, J. M. M.; Balbuena, P. B. Dealloying of Platinum-Based Alloy Catalysts: Kinetic Monte Carlo Simulations. *Electrochimica Acta* **2013**, *101*, 326–333. https://doi.org/10.1016/j.electacta.2013.01.053.

(155) Butler, J. a. V. Studies in Heterogeneous Equilibria. Part III. A Kinetic Theory of Reversible Oxidation Potentials at Inert Electrodes. *Trans. Faraday Soc.* **1924**, *19* (March), 734–739. https://doi.org/10.1039/TF9241900734.

(156) Yang, J. Atomic Simulations for Configurations and Solid-Liquid Interface of Li-Fe and Li-Cu Icosahedra. *J Nanopart Res* **2017**, 14.

(157) Selvaraj, C.; Munichandraiah, N.; Scanlon, L. Dilithium Phthalocyanine as a Catalyst for Oxygen Reduction in Non-Aqueous Li-O 2 Cells. *Journal of Porphyrins and Phthalocyanines* **2012**, *16* (03), 255–259.

(158) Sun, D.; Shen, Y.; Zhang, W.; Yu, L.; Yi, Z.; Yin, W.; Wang, D.; Huang, Y.; Wang, J.; Wang, D.; Goodenough, J. B. A Solution-Phase Bifunctional Catalyst for Lithium–Oxygen Batteries. *J. Am. Chem. Soc.* **2014**, *136* (25), 8941–8946. https://doi.org/10.1021/ja501877e.

(159) Hohenstein, E. G.; Chill, S. T.; Sherrill, C. D. Assessment of the Performance of the M05-2X and M06-2X Exchange-Correlation Functionals for Noncovalent Interactions in Biomolecules. *J Chem Theory Comput* **2008**, *4* (12), 1996–2000. https://doi.org/10.1021/ct800308k.

(160) Rivas, M. A.; Iglesias, T. P. On Permittivity and Density of the Systems (Tetraglyme+dimethyl or Diethyl Carbonate) and the Formulation of Δε in Terms of Volume or Mole Fraction. *The Journal of Chemical Thermodynamics* **2007**, *39* (12), 1546–1556. https://doi.org/10.1016/j.jct.2007.05.006.

(161) Olea, A. F.; Wilkinson, F. Singlet Oxygen Production from Excited Singlet and Triplet States of Anthracene Derivatives in Acetonitrile. *J. Phys. Chem.* **1995**, *99* (13), 4518–4524. https://doi.org/10.1021/j100013a022.

(162) Breneman, C. M.; Wiberg, K. B. Determining Atom-Centered Monopoles from Molecular Electrostatic Potentials. The Need for High Sampling Density in Formamide Conformational Analysis. *Journal of Computational Chemistry* **1990**, *11* (3), 361–373. https://doi.org/10.1002/jcc.540110311.

(163) Atkins, P. W.; Friedman, R. S. *Molecular Quantum Mechanics*; OUP Oxford, 2011.

(164) Sambasivarao, S. V.; Acevedo, O. Development of OPLS-AA Force Field Parameters for 68 Unique Ionic Liquids. *J. Chem. Theory Comput.* **2009**, *5* (4), 1038–1050. https://doi.org/10.1021/ct900009a.

(165) Jorgensen, W. L.; Maxwell, D. S.; Tirado-Rives, J. Development and Testing of the OPLS All-Atom Force Field on Conformational Energetics and Properties of Organic Liquids. *J. Am. Chem. Soc.* **1996**, *118* (45), 11225–11236. https://doi.org/10.1021/ja9621760.

(166) Leung, K.; Soto, F.; Hankins, K.; Balbuena, P. B.; Harrison, K. L. Stability of Solid Electrolyte Interphase Components on Lithium Metal and Reactive Anode Material Surfaces. *J. Phys. Chem. C* **2016**, *120* (12), 6302–6313. https://doi.org/10.1021/acs.jpcc.5b11719.

(167) Wi, S.; Shutthanandan, V.; Sivakumar, B. M.; Thevuthasan, S.; Prabhakaran, V.; Roy, S.; Karakoti, A.; Murugesan, V. In Situ X-Ray Photoelectron Spectroscopy Analysis of Electrochemical Interfaces in Battery: Recent Advances and Remaining Challenges. *Journal of Vacuum Science & Technology A* **2022**, *40* (1), 010808. https://doi.org/10.1116/6.0001460.

APPENDIX A

ADDITIONAL PROJECTS

A.1.[***]Stability of Solid Electrolyte Interphase Components on Lithium Metal and Reactive Anode Material Surfaces[166]

This was the first published project that I worked on. I began work on it during the second year of my undergraduate degree. In this project we used DFT calculations to examine the behavior of the initial layers of common SEI components (lithium carbonate, lithium ethylene dicarbonate, and lithium fluoride) on lithium-metal and lithium-silicon surfaces. In this project we were able to verify previously theorized behavior about the inner layers of the SEI. The aforementioned species are normally stable in the bulk of the SEI, but we determined that they will further decompose at the electrode interface to form lithium oxide and other organic fragments. This provides valuable insight on the heterogeneity of the initial stages of the SEI, and can guide the design of electrolytes and artificial surface coatings.

This was a collaborative work with Dr. Balbuena's group at the Texas A&M University Department of Chemical Engineering and Dr. Leung's group at Sandia National Lab.

[***] Reprinted with permission from "Stability of Solid Electrolyte Interphase Components on Lithium Metal and Reactive Anode Material Surfaces" by Kevin Leung, Fernando Soto, Kie Hankins, Perla B. Balbuena, and Katharine L. Harrison, 2016. J. Phys. Chem. C, 120, 6302-6313, Copyright 2016 by American Chemical Society.

A.2. †††Insights into the Li Intercalation and SEI Formation on LiSi Nanoclusters[146]

This was the second published project that I worked on, and my first first-authored publication. I began work on it during the third year of my undergraduate degree. In this project we used AIMD calculations to insert lithium atoms into a lithium-silicon nanocluster surrounded by ethylene carbonate in order to track the reaction pathways and initial stages of SEI formation of this formulation. We were able to develop a detailed map of the reaction pathways and illustrate the initial stages of the SEI network forming on a silicon surface.

This work was performed entirely by Dr. Balbuena's group at the Texas A&M University Department of Chemical Engineering.

A.3. KMC investigation of CaOH Dissolution in Concrete Structures

This is an ongoing project with Dr. Bullard's group at Texas A&M. We are using our KMC model in order to investigate the dissolution behavior of CaOH in concrete materials. This project will provide insight into the degradation modes industrial structures, and provides a great example of the robustness of our KMC model. We are using DFT and blue-moon AIMD to develop model parameters, and are adapting our code to better suit the mechanisms of mineral dissolution.

---

††† Reprinted with permission from "Insights into the Li Intercalation and SEI Formation on LiSi Nanoclusters" by Kie Hankins, Fernando A. Soto,1 and Perla B. Balbuena, 2017. J. Electrochemical Society, Volume 164, Copyright 2017 by IOP Publishing.

This is a collaborative work with Dr. Balbuena's group at the Texas A&M University Department of Chemical Engineering and Dr. Bullard in the Dr. Balbuena's group at the Texas A&M University Department of Civil Engineering.

A.4. Thermal Stability of ether-based solvents on Mg-metal surfaces

I worked on this project during my internship at PNNL. In this project we studied the thermal stability of several common solvents on magnesium surfaces. We performed XPS measurements at cryogenic conditions. This is an ongoing work that we hope to submit in the next few months.

This work was performed at PNNL under Dr. Vijay Murugesan's group.

A.5. In-situ XPS examination of cycling changes on aqueous Zn-based battery[167]

I assisted with this project during my internship at PNNL. In this project we used cryogenic XPS measurements in order to examine the reaction behavior of a Zn battery relative to reaction cycling. The cryogenic conditions allowed for the battery to be measured without removing the aqueous electrolyte, which allowed us to examine the battery in a more representative condition. We performed the measurements repeatedly at regular intervals during charging in order to examine the chemical changes that occurred. This project established a novel and effective way of observing the chemical changes of a battery system in response to charge cycling